

Influence of obstacles on urban canyon ventilation and air pollutant concentration: An experimental assessment

*Original*

Influence of obstacles on urban canyon ventilation and air pollutant concentration: An experimental assessment / Carlo, Os; Fellini, S; Palusci, O; Marro, M; Salizzoni, P; Buccolieri, R. - In: BUILDING AND ENVIRONMENT. - ISSN 0360-1323. - ELETTRONICO. - 250:(2024). [10.1016/j.buildenv.2023.111143]

*Availability:*

This version is available at: 11583/2991785 since: 2024-08-19T14:29:50Z

*Publisher:*

PERGAMON-ELSEVIER SCIENCE LTD

*Published*

DOI:10.1016/j.buildenv.2023.111143

*Terms of use:*

This article is made available under terms and conditions as specified in the corresponding bibliographic description in the repository

*Publisher copyright*

Elsevier postprint/Author's Accepted Manuscript

© 2024. This manuscript version is made available under the CC-BY-NC-ND 4.0 license  
<http://creativecommons.org/licenses/by-nc-nd/4.0/>. The final authenticated version is available online at:  
<http://dx.doi.org/10.1016/j.buildenv.2023.111143>

(Article begins on next page)



# Influence of obstacles on urban canyon ventilation and air pollutant concentration: An experimental assessment

Oliver S. Carlo<sup>a</sup>, Sofia Fellini<sup>b,c</sup>, Olga Palusci<sup>a</sup>, Massimo Marro<sup>b</sup>, Pietro Salizzoni<sup>b,c</sup>, Riccardo Buccolieri<sup>a,\*</sup>

<sup>a</sup> Dipartimento di Scienze e Tecnologie Biologiche ed Ambientali, University of Salento, Laboratory of Micrometeorology, 73100, Lecce, Italy

<sup>b</sup> Univ Lyon, Ecole Centrale de Lyon, CNRS, Univ Claude Bernard Lyon 1, INSA Lyon, LMFA, UMR5509, 69130, Ecully, France

<sup>c</sup> Department of Environmental, Land and Infrastructure Engineering, Politecnico di Torino, 10129, Turin, Italy

## ARTICLE INFO

### Keywords:

Passive methods  
Pollutant dispersion  
Urban canyon  
Obstacles  
Air quality  
Urban planning

## ABSTRACT

Air pollution in cities, intensified by vehicular traffic emissions and reduced ventilation, poses a significant health risk. Obstacles, like solid or vegetation barriers, are being considered as strategies to reduce pollution exposure for pedestrians and nearby residents in street canyons. This study utilises wind tunnel experiments, to simulate a typical urban canyon with street intersections on both sides, in a 1:200 scale and an  $H/W = 0.5$ , positioned perpendicular to the free stream wind flow. A passive scalar representing a vehicular pollutant is released along the length of the street canyon. Concentration measurements inside the canyon are performed to determine the effect of parked cars, boundary walls, hedges and trees on pollutant concentration exposure for pedestrians on the sidewalk. Results show that one circulating vortex is generated within the canyon, driving the pollutant to accumulate along the leeward (upwind) wall. Tightly parked cars, boundary walls and hedges, placed along the sidewalk near the leeward wall, can reduce pedestrian pollutant exposure by 15 %, 23 % and 11 % respectively along this sidewalk. Attributes such as obstacle height, surface roughness and porosity play a key role in their performance. However, trees, when placed in the same area, increase pedestrian pollutant exposure by 51 % and 17 % under dense and sparse tree arrangements, respectively. While a broader analysis that considers the variability of vegetation attributes (e.g., porosity, stand density) is desirable, this study remains crucial for validating numerical simulations and suggesting optimal urban measures to reduce pollution exposure for citizens.

## 1. Introduction

Air pollution is a serious concern for public health in urban areas worldwide, with both gaseous and particulate matter (PM) pollution having detrimental effects on human health. The Organisation for Economic Cooperation and Development estimates that the concentration of PM in the air is particularly concerning, as it is responsible for over 1 million premature deaths annually, which is expected to increase to 3.6 million per year by 2050 [1]. Most of these deaths are projected to occur in countries such as India and China, where urbanisation and industrialisation have resulted in significant air pollution [1].

Among gaseous pollutants, nitrogen oxides (NO<sub>x</sub>) are a significant group of pollutants that threaten air quality in urban environments. These emissions encompass nitrogen dioxide (NO<sub>2</sub>), which can have detrimental effects on respiratory health and lung function when

individuals are exposed to high concentrations. It weakens the body's defences against respiratory infections, such as pneumonia and influenza [2].

Urban air pollution sources include both anthropogenic and natural factors [3]. Anthropogenic sources are emissions from road transport, industries, and domestic heating, while natural sources include dust storms, wind erosions, and wildfires [3]. In urban areas, the concentration of pollutants is intensified due to their unique form and structure, creating street canyons that trap pollutants within them [4].

One of the primary contributors to air pollution in urban canyons is vehicular traffic, and areas with high traffic volumes have significantly higher pollutant concentrations. This poses severe health hazard risks for pedestrians and building residents on lower floors facing streets with higher pollutant concentrations [4]. To address this issue, literature review studies have highlighted passive design strategies to mitigate

\* Corresponding author.

E-mail address: [riccardo.buccolieri@unisalento.it](mailto:riccardo.buccolieri@unisalento.it) (R. Buccolieri).

roadside air pollution in urban canyons [5–13]. Some strategies include urban morphological design and building typology changes that are more suited for new developments. However, more widely applicable strategies, especially in existing urban areas, include the study and use of obstacles for altering the flow of pollutants from vehicles to pedestrians [5,8,14].

Obstacles in street canyons can be defined as an obstruction to the airflow that occurs over and above other pertinent urban installations such as buildings and streets [10]. These include parked cars, boundary walls, hedges, and trees, which have shown potential to change pollutant dispersion patterns and reduce pollutant concentrations within street canyons [5,8,10]. Implementing obstacles in street canyons is an affordable and accessible solution for policymakers and communities, making it more feasible than structural modifications to the urban layout [8]. However, the effectiveness of obstacles depends on factors like local meteorological conditions, pollutant type, pollutant concentration levels, and urban morphology [8,10,11].

While large obstacles like trees can affect the pollutant dispersion within the entire street canyon [15], smaller obstacles like cars and boundary walls are expected to impart most benefit for the pedestrian breathing zone (e.g., along sidewalks) [9]. The pedestrian zone lies within 1.5 m above ground level and warrants greater priority in an urban canyon from a pollutant exposure perspective. Therefore, it is essential to conduct investigative studies assessing the performance of obstacles in this zone, to guide better decision-making processes and reduce the necessity for trial-and-error [8].

The investigation of obstacle impact on flow patterns within an urban canyon can be conducted through various methods. These include full-scale field measurements, reduced-scale wind tunnel (WT) experiments, and computational fluid dynamics (CFD) simulations. Field measurements are considered the gold standard but have drawbacks such as limited sampling points and concentration patterns, which are subject to the influence of unsteady meteorological conditions or vehicular-motion induced localised turbulence [16,17]. WT experiments offer better control over the initial and boundary conditions replicating meteorological phenomena for urban areas. Moreover, measurements can be conducted at more sampling points than with respect to field studies. However, WT experiments require adherence to specific similarity criteria (e.g., Rossby, Reynolds, Froude and Peclet numbers of governing equations) to ensure similarity between the reduced WT scale and the full-scale models [18,19]. CFD simulation techniques allow full control over initial and boundary conditions, analysis of whole-field flow data, and can be modelled in full-scale. However, reliability and accuracy are important concerns [18,20]. Therefore, WT experimental data are crucial for verifying and validating CFD studies [18,21,22].

This study makes a valuable contribution to the research field by addressing several key aspects. For instance, while previous studies have investigated the effect of single obstacles, almost none have provided wind tunnel experimental data comparisons for different obstacles with the same urban morphology and atmospheric boundary layer. WT studies by Heist et al. [23] explored different roadway configurations using only one obstacle, i.e. boundary walls. Fellini et al. [15] experimented with three different tree configurations, while Gromke et al. [24, 25] utilised a single tree configuration to study the concentration and velocity fields in a street canyon. Parked cars were investigated through some field studies and CFD simulations [26–28], but no wind tunnel study was found. Comparisons across different obstacles is necessary as the flow around them presents different investigative challenges, with porous/vegetative barriers being inherently more complex compared to solid barriers and giving rise to the development of boundary layers [29, 30].

Porous obstacles, especially trees, are complex, because studies show conflicting evidence for the effects the different tree variables have on air pollution in urban areas. Factors such as stand density, arrangement, crown porosity, and leaf area density (LAD) differently influence pollution concentration levels [11,12,31–34]. Couple of field studies

show that the aerodynamic effect of trees typically has a more significant impact than the deposition effect, causing a worsening of pollutant concentration in street canyons [35,36], with trees more likely to have a “trapping” effect in restrictive/deeper street canyons [37]. However, this trapping effect may be beneficial along open road conditions (e.g., freeways), as a couple of field studies demonstrate that dense, tall, and low-porosity vegetation, further assisted when combined with noise barriers, yielded better air quality for the surrounding neighbourhoods [38,39]. Comprehensive reviews by Abhijith et al. [11] and Kumar et al. [12] examined the air pollution abatement performance of green infrastructure and its impact on human health, deducing that open road conditions could benefit from generic recommendations for vegetated barriers, but built-up street canyons should have tailored design guidelines measuring the specific air quality health benefits they provide. In line with this, the review by Janhäll [40] indicates the need for well-structured experimental data of porous vegetated media and detailed empirical descriptions of parameters, with Buccolieri et al.’s [32] review noting that numerical studies continually seek better ways of parametrising porous media variables associated with the momentum, turbulent kinetic energy (TKE) production and dissipation rate, particle deposition and resuspension, and thermal effects. This paper aims to dig deeper into these aspects, as strengthening our understanding of dispersion parametrization rests on the availability of wind tunnel studies investigating porous vegetated media in urban canyons.

Non-porous obstacles are less complex than porous media, primarily aiding in the control of pollutant source-receptor pathways in an urban canyon [8,28,41]. In this instance, the obstacles act as barriers that alter the pathways between the vehicular pollutant (source) and the pedestrians along the sidewalk (receptor). Hence parked cars and boundary walls are shown to have the maximum effect on pedestrian pollutant exposure near the street level [26,33]. But compared to the literature on porous vegetated obstacles, far fewer studies are found for non-porous obstacles, and most are CFD-based [10]. Height of the obstacles are an important variable in reducing concentrations behind the barrier [42, 43], playing an important role in open road conditions and rural-to-urban wind transitions [14]. However, the same cannot be said for urban canyons, as the height of obstacles is constrained for aesthetic reasons. Apart from the height, the shape of non-porous obstacles may encourage lower pollution exposure for pedestrians in urban canyons [44,45], and reasonably resolving these shapes in CFD simulations is also important [26]. This should also be comparable to altering the surface roughness of the obstacle as supported by other studies [46,47]. Typically, the variables of low-level obstacles (like height, shape, surface roughness) have the potential to alter the velocity vectors and vortex structures near the obstacle, inducing minor eddies at street corners, which should alter the pollutant dispersion patterns [48,49]. The CFD study by Wang et al. [48] also found that changing wind speeds expanded or compressed the vortices and eddies within the canyon in the presence of low boundary walls. Unfortunately, very few studies address these aspects further, and this study aims to delve deeper into them.

The findings will shed light on the specific advantages and variables associated with each obstacle that affect pollutant dispersion in an urban canyon. Moreover, numerical simulations are commonly validated against reference empty street canyons or those with a single obstacle type. Through experimental investigation of various obstacle types under consistent urban morphology and meteorological conditions, this study enhances the evidence-base for future numerical and computational studies. This will provide practitioners and researchers with reliable validation data. The insights from this study should provide useful perspectives for policymakers, urban planners, and researchers, potentially informing their approach to implementing obstacle-based strategies for improving air quality and protecting the health of pedestrians in urban environments.

## 2. Methodology

The atmospheric closed-circuit wind tunnel at the Laboratoire de Mécanique des Fluides et d'Acoustique (LMFA) at the Ecole Centrale de Lyon was used to conduct the experiments. The experimental setup resembled that of previous studies that also utilised the same wind tunnel facility [15]. The axial fan of the aerodynamic circuit generated wind velocities between 0.5 and 6 m per section ( $\text{ms}^{-1}$ ), and the air temperature was regulated by a heat exchanger system with a precision of 0.5 K (K). The test section of the wind tunnel measured 12 m (m) in length, 3.6 m in width, and 2 m in height [15].

To model the vehicular pollutant source within a typical street canyon, a line source emitting an ethane tracer (pollutant) was aligned along the centre of the canyon, while the pedestrian walkways zones were modelled along the sidewalks close to the walls of the buildings. The study modelled a flat roof geometry, with the ambient wind direction perpendicular to the street canyon, as many studies report this to be the worst-case street configuration for the dispersion of pollutants causing high levels of wind stagnation and accumulation of pollutants [10,50].

### 2.1. Physical model

#### 2.1.1. Urban setting

To simulate the turbulent flow within and above an idealised urban district, an array of square blocks made of wood and polystyrene, measuring 50 cm (cm) in length ( $L$ ) and 10 cm in height ( $H$ ), was overlaid on the floor of the entire test section (see Fig. 1). The blocks were spaced 10 cm span-wise and 20 cm lengthwise ( $W$ ) from each other, to create a network of street canyons with a height-to-width ratio

of  $H/W = 1$  in the street canyons aligned with the wind direction and  $H/W = 0.5$  in the larger streets perpendicular to the wind direction, respectively. The blockage ratio of the model to the cross-section of the wind tunnel was 5 % [15].

The reference street canyon used in the study was located around 8 m away from the start of the test section, in one of the streets perpendicular to the wind direction and centrally located along the width of the WT. It measured 0.5 m in length ( $L$ ), 0.2 m in width ( $W$ ), and 0.1 m in height ( $H$ ), resulting in aspect ratios of  $H/W = 0.5$ ,  $L/H = 5$ , and  $L/W = 2.5$  (Fig. 1a). This geometry is representative of a typical tree-lined boulevard measuring 40 m in width with 20 m high buildings on a 1:200 scale, as seen in typical European city centres such as Barcelona, Turin, or Lyon [15].

A neutrally stratified boundary layer approximately 1.1 m depth was generated by combining the effect of a row of 0.95 m high Irwin spires [51], placed at the beginning of the test section, and the building-like obstacles on the floor. Moreover, the obstacles were covered by 5 mm (mm) high nuts to generate further roughness and accelerate the full development of the boundary layer. The free stream velocity at the top of the boundary layer ( $U_\infty$ ) was kept constant at  $5 \text{ ms}^{-1}$ . See also Fellini et al. [15] for further details about the experimental setups.

#### 2.1.2. Obstacle scenarios

To simulate each of the obstacles presented in the Introduction (see Section 1), a 1:200 scale was designed to match it with the experimental setup. The different urban street canyon scenarios considered are as given below:

- Case R – Reference case scenario with no obstacles.
- Case PC – Parked cars along the pedestrian sidewalk.
- Case BW – Boundary walls along the pedestrian sidewalks.

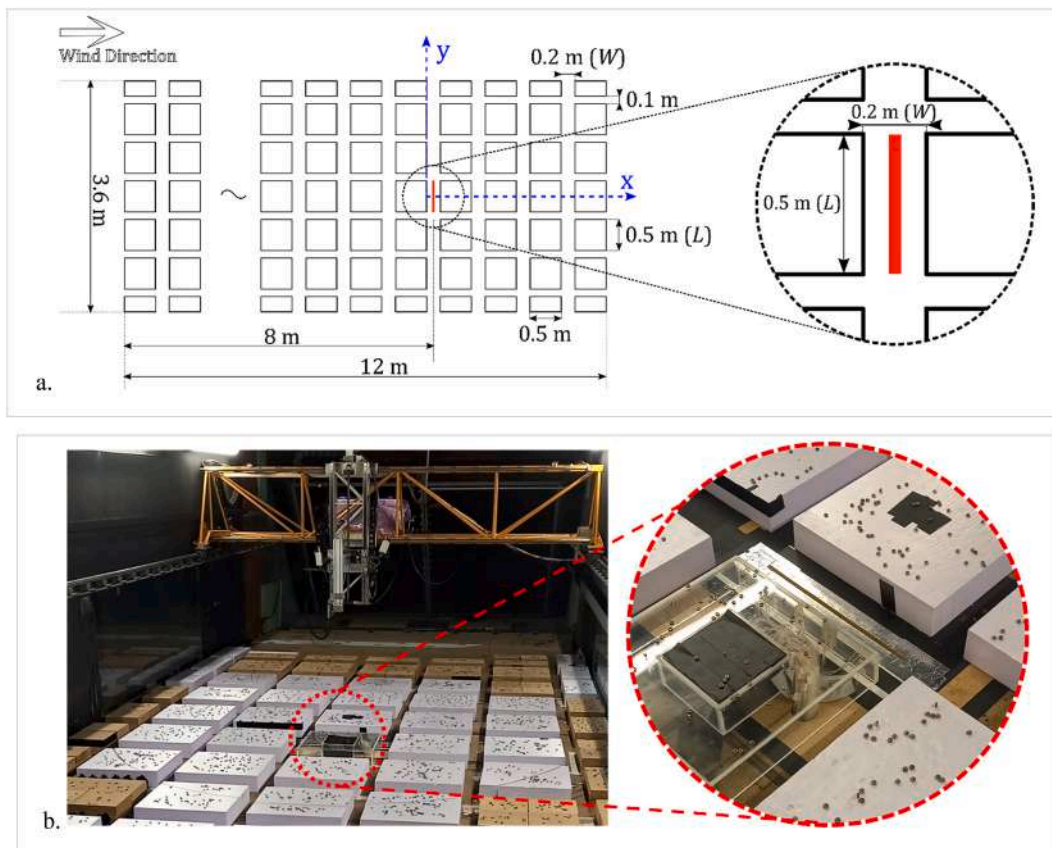


Fig. 1. (a) Sketch showing the top view of the urban canopy experimental setup in the wind tunnel with a zoomed view of the area of interest, showing the position of the ethane tracer in red. Adapted from Fellini et al. [15]. (b) Photo of the general experimental setup in the wind tunnel. (For interpretation of the references to colour in this figure legend, the reader is referred to the Web version of this article.)

Case H – Hedges along the pedestrian sidewalks.

Case TD – Trees (dense) along the pedestrian sidewalks.

Case TS – Trees (sparse) along the pedestrian sidewalks.

The sketch of each case setup is shown in Fig. 2 along with the obstacle dimensions. Photographs of the obstacles are shown in Fig. 3.

## 2.2. Similarity criteria

### 2.2.1. Characterisation of urban boundary layer

The turbulent boundary layer above the urban canyon was characterised by measuring and focusing on the statistical properties of the turbulent flow. For this, vertical velocity profiles were measured near the urban canyon.

The evolution of the boundary layer, and verification of the fully developed profiles was recorded for the same wind tunnel and urban canopy by Fellini et al. [15] to which we refer for further details. Since the experimental setup and inlet conditions remained unchanged in our study, a thorough assessment of the boundary layer's development across the entire wind tunnel fetch was not repeated. Nevertheless, to confirm that the boundary layer conditions had not changed from the previous experiment, we conducted measurements of vertical velocity profiles at four locations near the reference canyon (above a building roof, above the reference horizontal canyon, above a lateral street canyon, and above a street intersection) to account for horizontal variations. Fig. 4 illustrates these measurements, including an error bar representing the standard deviation derived from the four profiles. The measurements were performed with a Hot-Wire Anemometer (HWA) at constant temperature, with an X-wire probe with an acceptance angle of 45°, which allowed measuring two velocity components of the velocity field simultaneously. A platinum probe wire 1 mm long with a diameter of 5  $\mu\text{m}$  ( $\mu\text{m}$ ) was used, and the low thermal inertia of the material ensured fast response, allowing the detection of high-frequency fluctuations of the turbulent flow [52]. An acquisition time of 1 min at a frequency of 4000 Hz was adopted for each sampling point. Calibration of the HWA was carried out by using a Pitot tube to measure a reference velocity [53,54]. The HWA was not sensitive to capture the velocity field within the urban canyon, so only velocity measurements above the buildings were captured to characterise the approaching flow.

The mean horizontal velocity in Fig. 4a shows that the free-stream velocity was  $U_\infty = 5 \text{ ms}^{-1}$  while the height of the boundary layer was  $\delta = 1.1 \text{ m}$ . The ratio of  $\delta/H = 11$  is in the typical range of  $\delta/H \approx 10 - 20$  for atmospheric flow over urban canopies [55].

The vertical profile of the mean horizontal velocity  $U$  [ $\text{ms}^{-1}$ ] above the urban canopy is obtained using the logarithmic law given in Equation (1), first introduced by Richards and Hoxey [56]:

$$U(z) = \frac{u^*}{\kappa} \ln \frac{z-d}{z_0} \quad (1)$$

where  $\kappa = 0.4$  is the von Kármán constant,  $z_0$  is the aerodynamic roughness length,  $d$  is the zero-plane displacement, and  $u^*$  is the friction velocity. The values of these parameters were found by Fellini et al. [15] using two different methods for fitting the experimental data:  $u^* = 0.29 \text{ m/s}$  ( $u^*/U_\infty = 0.051$ ),  $d = 0.094 \text{ m}$  ( $d/\delta = 0.085$ ),  $z_0 = 1 \times 10^{-3} \text{ m}$  ( $z_0/\delta = 9 \times 10^{-4}$ ). Similar values for WT experiments were reported in other studies [57–60] and are in the reasonable range of variation proposed by Grimmond and Oke [61]. Also, the scaled velocity standard deviations are in line with the field measurements proposed by Rotach [62].

While the logarithmic law is suitable for modelling the inertial layer, a good fit of the mean velocity profile in the whole turbulent boundary layer (Fig. 4a) can be obtained by a power law [57] of the form:

$$\frac{U(z)}{U_\infty} = \left( \frac{z-d}{\delta-d} \right)^n \quad (2)$$

where the exponent  $n$  was found to be 0.21.

The trend of Reynolds stresses along the vertical axis, shown in Fig. 4b, aligns with previous experimental studies concerning boundary layers over urban canopies [60,63,64]. It shows the vertical profile of the Reynolds stresses. The error bars (i.e., the standard deviation of the measured four vertical profiles) reveal the high horizontal heterogeneity of the velocity field within the so-called roughness sub-layer, which in this study extends up to  $z/H = 0.3$  [15]. The description of the boundary layer is employed by averaging four vertical profiles, taken over four different horizontal positions, details of which can be found in Fellini et al. [15].

For turbulence closure in CFD simulations, these Reynolds stresses are modelled using an effective turbulent viscosity  $\mu_t$  which is related to the turbulent kinetic energy (TKE)  $k$  [ $\text{m}^2\text{s}^{-2}$ ] and TKE dissipation rate  $\epsilon$  [ $\text{m}^2\text{s}^{-3}$ ] (e.g., the RANS  $k - \epsilon$  model). These quantities ( $k$  and  $\epsilon$ ) can be calculated from the HWA experimental data using Equation (3) and Equation (4) respectively [56]:

$$k = \frac{1}{2} (\overline{u^2} + \overline{v^2} + \overline{w^2}) \quad (3)$$

$$\epsilon = \frac{15\nu}{U^2} \left( \frac{\partial u}{\partial t} \right)^2 \quad (4)$$

In particular, Equation (4) is based on the isotropic approximation and Taylor's hypothesis of frozen turbulence [65–67]. The vertical

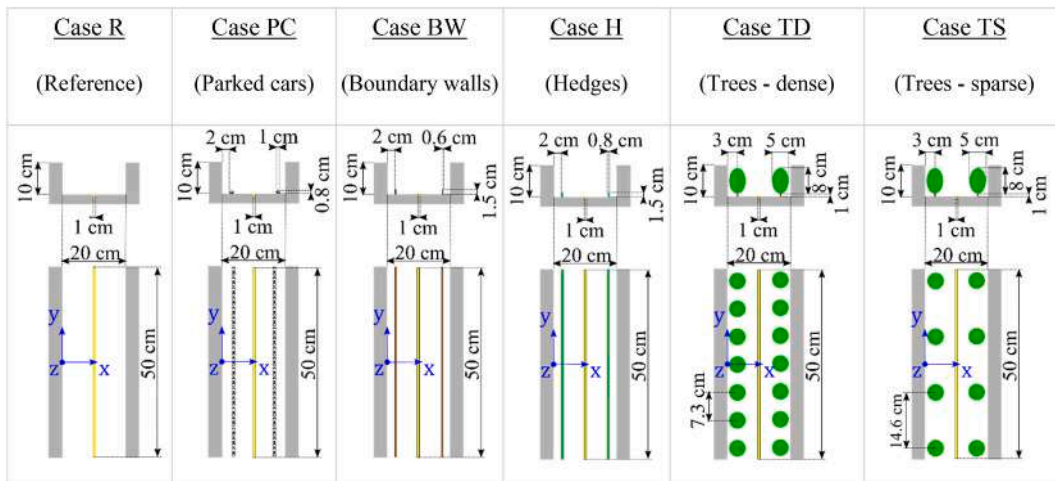
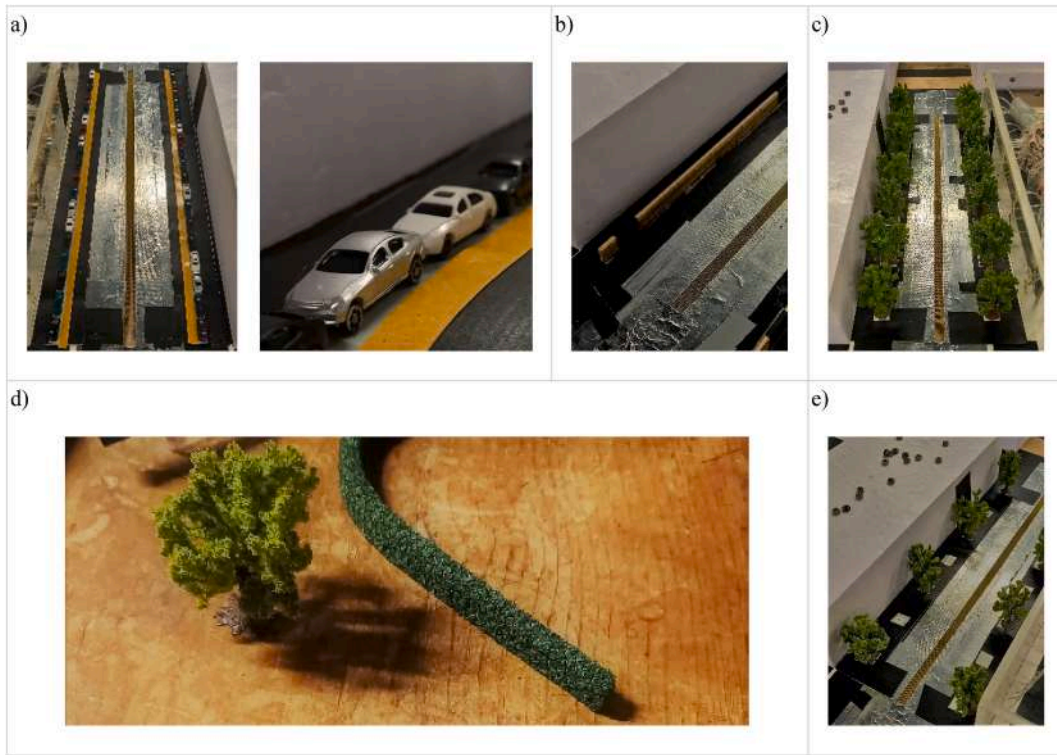


Fig. 2. Sketches of each of the experimental scenarios investigated in the wind tunnel.



**Fig. 3.** Photographs of the obstacles used in the investigated experimental scenarios. (a) Miniature parked cars; (b) miniature boundary walls; (c) dense trees arrangement in street canyon; (d) miniature hedges and a single tree (photo taken out of the investigated test scenario); (e) sparse trees arrangement in street canyon.

profiles of  $k$  and  $\epsilon$ , obtained from the velocity measurements, are shown in Fig. 4c and d, respectively. The production rate of TKE is also reported in Fig. 4d and is estimated as  $P = -\overline{uw} \frac{\partial U}{\partial z}$  [15,57,64]. The other eight components of the production rate of TKE are negligible, since the average vertical and transverse velocities are null (i.e.,  $V = 0$ , and  $W \ll U$  considering boundary layer approximation for the fully developed flow profile [15]), and the derivatives of horizontal velocity along the wind tunnel fetch (x-axis) and across the transverse y-axis are negligible (i.e.,  $d/dx$  and  $d/dy$  are zero). The good agreement between  $P$  and  $\epsilon$  profiles confirm that, for most of the boundary layer, the production and dissipation rate of turbulent kinetic energy are in local equilibrium, which is a prerequisite for the logarithmic boundary layer profile [56, 57].

### 2.2.2. Characterisation of obstacles

To investigate the effects of obstacles in urban areas through wind tunnel experiments, buildings, obstacles, and vegetative structures need to be modelled on a reduced scale since the size afforded by wind tunnel facilities cannot mimic large neighbourhoods and cities with a 1:1 ratio. To ensure that the results of scaled models are applicable to the real scale, both geometric and dynamical similarity must be achieved.

For impermeable and rigid structures like buildings, the dynamical similarity between the experiment and the real application exists if the reduced-scale model and the full-scale object are geometrically similar and the two flows have the same Reynolds number.

The characteristic Reynolds numbers for this experiment are  $Re_\infty = (U_\infty H)/\nu \approx 33,000$  and  $Re_H = (U_H H)/\nu \approx 12,500$ , where  $H$  is the obstacle height,  $\nu$  the kinematic viscosity of the fluid,  $U_\infty = 5 \text{ ms}^{-1}$  is the free stream velocity and  $U_H = 1.94 \text{ ms}^{-1}$  is the mean horizontal velocity at  $z = H$ . In an isolated quasi-2D street canyon study, Marucci and Carpentieri [68] found that for Reynolds numbers based on the wind speed at the building height ( $Re_H = U_H H/\nu$ ) exceeding 4000, there were no observable Reynolds number effects for the flow field within a street canyon of unit aspect ratio ( $H/W = 1$ ). Considering a Reynolds number

based on the free-stream velocity ( $Re_\infty = U_\infty H/\nu$ ), a quasi-2D cavity study by Allegrini et al. [69] established Reynolds-independent flow within a square cavity for  $Re_\infty$  surpassing 13000. The experimental configuration under investigation in this study is characterised by Reynolds numbers approximately three times higher than the previously mentioned critical thresholds. Additionally, the canyon is twice as wide (or to be more precise, has a halved  $H/W$  aspect ratio) as compared to the referenced studies. These details provide assurance that fully developed turbulent flow conditions are present within the urban canyon under study. The presence inside the street canyon of large obstacle as trees, however, could significantly alter the velocity field, particularly in their immediate vicinity. While the elevated Reynolds number values in this experiment suggest that, despite the velocity reduction induced by the trees, the flow field can still be considered fully turbulent within the canyon, it's worth noting that a more definitive assessment of Reynolds number independence in the presence of vegetation would entail replicating the experiment under varying external wind intensities. This aspect was not addressed in the current study, but it presents an interesting prospect for future research.

Turning instead to the dynamic similarity of porous materials, previous studies suggest two key parameters to compare natural and model trees, i.e., the drag coefficient ( $c_d$ ) and the aerodynamic porosity ( $\alpha_p$ ) [15,70–72]. Aerodynamic porosity ( $\alpha_p$ ) [15,70] is defined as the ratio of the time average wind speed behind the obstacle ( $U_b$ ) and the average speed of the approaching wind ( $U_{ref}$ ):

$$\alpha_p = \frac{\int_{A_c} U_b(x, y) dA_c}{\int_{A_c} U_{ref}(x, y) dA_c} \quad (5)$$

where ( $A_c$ ) is the projected frontal area of the obstacle. Hence, aerodynamic porosity determines the portion of the flow that passes through the porous material with respect to the flow that diverges from the obstacle. The drag coefficient ( $c_d$ ) [15,70] is defined as:

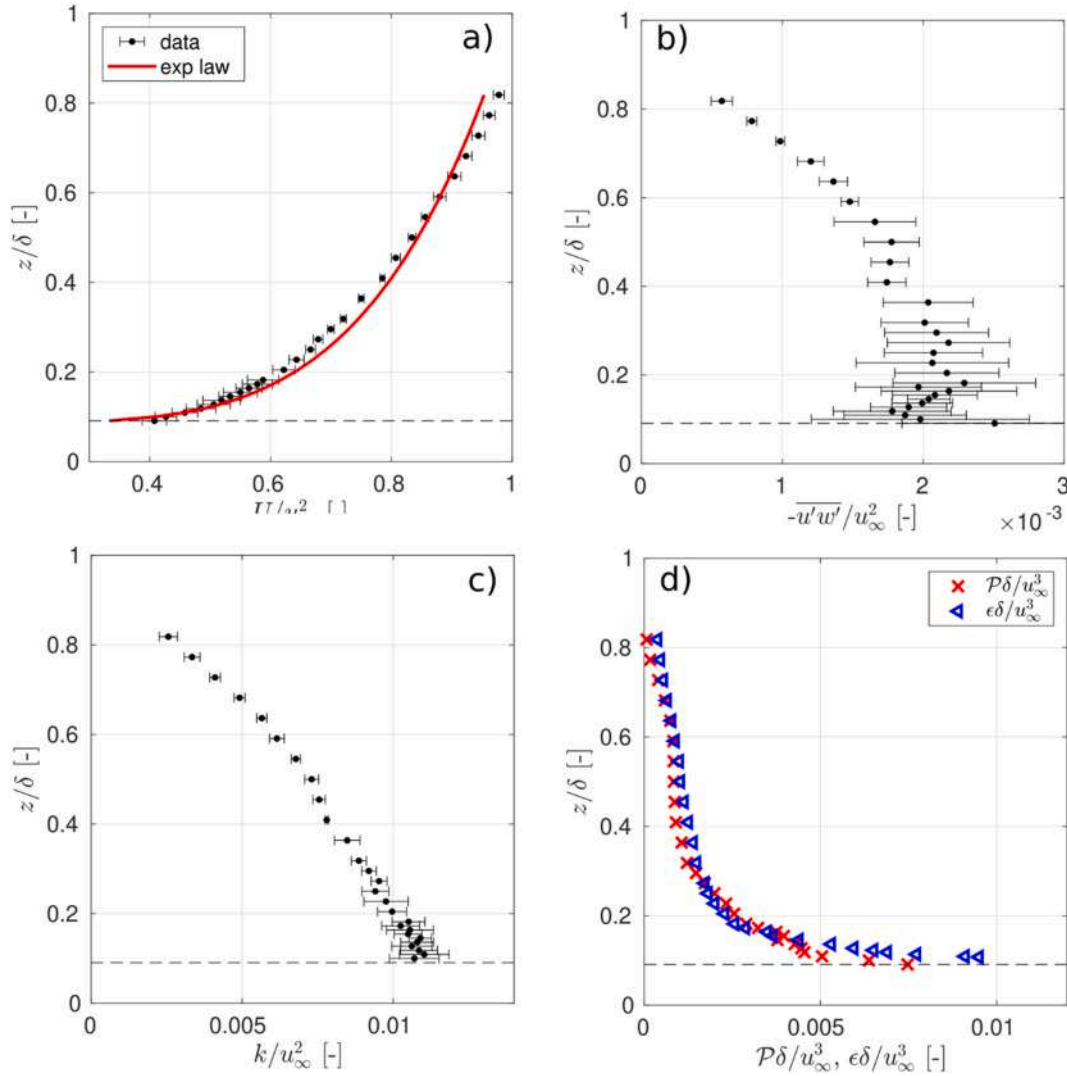


**Fig. 4.** (a) Mean velocity obtained as average of four different positions. The line represents the power-law as given by Equation (2). (b) Reynolds stresses  $-\overline{u'w'}$ . (c) Turbulent kinetic energy (TKE). (d) Production and dissipation rate of TKE. Figures (a), (b) and (c) also show the horizontal error bars representing the standard deviation  $\pm 1\sigma$ . Images taken and adapted from Fellini et al. [15].

$$c_d = \frac{2F}{\rho_a U_{ref}^2 A_c} \quad (6)$$

where  $F$  is the drag force in Newton [N],  $\rho_a$  is air density  $\approx 1.2 \text{ kg m}^{-3}$  at  $20^\circ$  centigrade ( $^\circ\text{C}$ ),  $U_{ref}$  is the reference velocity [ $\text{ms}^{-1}$ ] for the approaching wind, and  $A_c$  is the projected frontal area of the obstacle [ $\text{m}^2$ ]. For the aerodynamic characterisation of the model trees, the same data used by Fellini et al. [15] was employed. The drag coefficient ( $c_d$ ) was measured in a small closed-circuit wind tunnel with a  $30 \text{ cm} \times 30 \text{ cm}$  test section, capable of generating velocities up to  $25 \text{ ms}^{-1}$ . The tunnel was equipped with an external load cell with a precision of 0.01 N. Different layouts of trees were attached to a removable plate connected with the load cell, and the drag coefficient was estimated for varying wind velocities inside the tunnel. Moreover, the aerodynamic porosity of the model trees was evaluated by performing velocity measurements on the windward and leeward side of a single tree on a regular grid of points. A Pitot tube was used for measuring the average velocity since only the measurement of the average velocity was needed [15].

Using Equation (5), an aerodynamic porosity of  $\alpha_p \approx 0.3$  was obtained for the trees in this study, a value that is in line with that of common natural trees such as hollies and cypresses [15]. Using Equation (6), the drag coefficient was found to rapidly converge to a value of  $c_d \approx$

0.65, and this value is in line with the drag coefficient of natural trees, confirming that the model trees adopted for this study present realistic aerodynamic properties [15].

From Fig. 5a, the drag measurements for wind speeds below  $5 \text{ ms}^{-1}$  appear to exhibit significant uncertainty, primarily attributed to the precision of the load cell used to measure drag force. With an accuracy of 0.01 N for measured drag forces of approximately 0.02/0.03 N at  $4 \text{ ms}^{-1}$  wind speed, this factor can explain the non-constant behaviour of the drag coefficient at lower wind speeds. We also note that the drag coefficient of the tree is measured under conditions that differ from those in the experiment. Specifically, the drag force is assessed for a single tree exposed to a free flow, as opposed to a tree situated within a row of trees inside a street canyon with recirculating wind. This approach was chosen with the objective of characterising the individual tree to compare it with other vegetation (as shown in Fig. 5b), whose aerodynamic properties were measured under similar conditions. But as Zhao et al. [73] has noted, achieving similarity for vegetation (like trees) within a street canyon is a complicated issue and remains an open question in the scientific literature. Regardless, the aerodynamic characterisation of vegetation, using two crucial fluid dynamics parameters such as drag coefficient and aerodynamic porosity, lends significant credence for comparison with numerical CFD simulations.

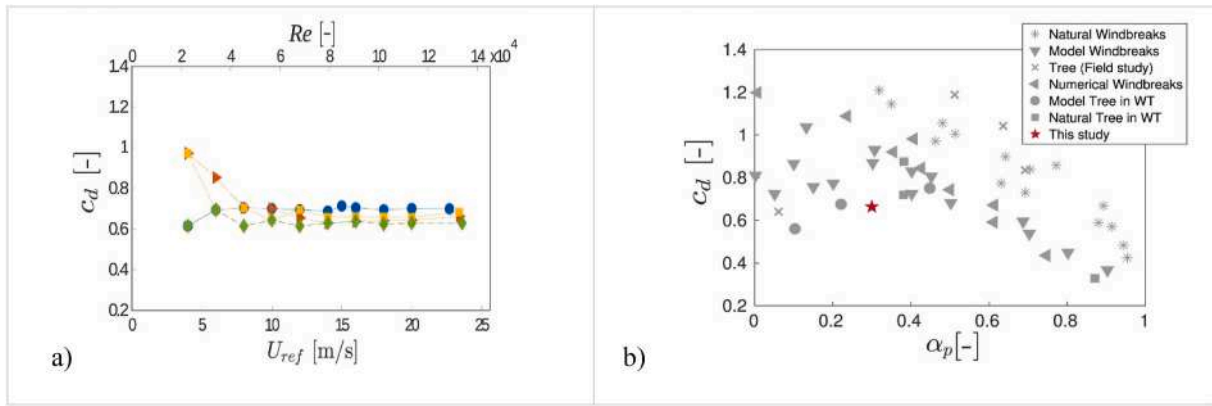


**Fig. 5.** (a) Drag coefficient obtained for the model tree as a function of wind velocity and Reynolds number, for four different alignments (rotating a single model tree on its vertical axis by 90°) reported by four different colours. Taken from Fellini et al. [15] (b) Drag coefficient and aerodynamic porosity for various model trees and natural trees. Taken from Manickathan et al. [72]. (For interpretation of the references to colour in this figure legend, the reader is referred to the Web version of this article.)

For hedges, the pressure loss coefficient  $\lambda$  [ $\text{m}^{-1}$ ] was estimated, as suggested by previous studies [31,32,35,37]:

$$\lambda = \frac{\Delta p_{stat}}{\rho_{dyn} d} = \frac{P_{windward} - P_{leeward}}{\frac{1}{2} \rho u^2 d} \quad (7)$$

where  $\lambda$  is the ratio between the static pressure difference between the windward and leeward side of the porous material  $\Delta p_{stat}$  [Pa] and the dynamic pressure divided by stream-wise depth of the material  $d$  [m]. This parameter is closely related to the drag coefficient  $C_d$ , as  $\lambda = LADC_d$ , where LAD [ $\text{m}^2\text{m}^{-3}$ ] is the leaf area density of the vegetation. The pressure drop coefficient was estimated by adopting the same technique reported in Gromke [30] to measure the pressure loss through the hedges. A flow of 20 L per minute ( $\text{L min}^{-1}$ ) was generated inside a circular plastic tube with diameter 2.54 cm (cm) (or 1 inch), thus generating an average wind speed of  $0.66 \text{ ms}^{-1}$ . A cross-section of the tube was entirely filled with the hedges of thickness  $d = 0.8$  cm. A manometer was used to measure the pressure difference before and after the hedges.

From the experiment, the values obtained were  $\Delta p_{stat} = 8.5$  Pa,  $d = 0.8$  cm and  $u = 0.66 \text{ ms}^{-1}$ . Substituting these values in Equation (7), the pressure loss coefficient was obtained as  $\lambda \approx 4000 \text{ m}^{-1}$ . Applying the similarity criterion as shown by Gromke [30], this pressure loss coefficient result can be transferred to a full-scale model, denoted as  $\lambda_{fs}$ , using the 1:200 scale of the WT setup. In this case,  $\lambda_{fs} \approx 20 \text{ m}^{-1}$  for a full-scale model, which can be realistically compared against a dense bird-cherry vegetated shelter belt (genus *Prunus padus*) commonly employed for urban plantings [29,74,75].

The results obtained from these standalone experiments, while useful for the characterisation of the porous obstacles, cannot be directly transferred to the analysis of the flow within the studied street canyon due to the changes in configuration and flow field, and must be applied

with caution in CFD studies.

### 2.3. Pollution modelling

#### 2.3.1. Vehicular emission source design

To simulate vehicular emissions, a tracer was released at street level from a linear source at the centre of the reference street canyon. The source, with its design details shown in Fig. 6, consisted of a metallic tube pierced with capillary needles emitting ethane in a gas homogenisation chamber of cavity size  $1 \text{ cm} \times 1 \text{ cm} \times 65 \text{ cm}$  [76]. From this chamber, the gas was emitted at street level from a 50 cm long and 1 cm wide metallic grid. The source emission length was chosen to be exactly the length of the street canyon ( $L$ ) and not pass through the canyon intersections to avoid any lateral entrainment of the tracer that would disrupt the uniformity of flow within the street canyon. The system was designed to minimise the vertical momentum and maximise the lateral homogeneity of the emission, following the indications of Meroney et al. [77]. The gas emission consisted of a mixture of air and ethane, with ethane serving as a passive tracer detectable by the Flame Ionization Detector (FID) having a density ratio of approximately 1.03 compared to air. The total air-ethane flow rate was  $4.0 \text{ L min}^{-1}$ , with a percentage of ethane of 1.25 % in volume ( $0.05 \text{ L min}^{-1}$ ). The injection velocity at the street level was around  $0.013 \text{ ms}^{-1}$ . The supply of the two gases was regulated by two digital mass-flow controllers (Alicat Scientific MC-Series) operating in a range between 0.1 and 20 normal litres per minute ( $\text{NL min}^{-1}$ ) for air and 0.01 and  $2 \text{ NL min}^{-1}$  for ethane, with an accuracy of 0.5 % [15].

The small diameter of the capillary needles produces a significant pressure drop. This renders the gas flow insensitive to local pressure fluctuations in the model street canyon above the line source and to pressure variations within the tubes. To confirm the uniformity of emission, preliminary concentration measurements were taken in the

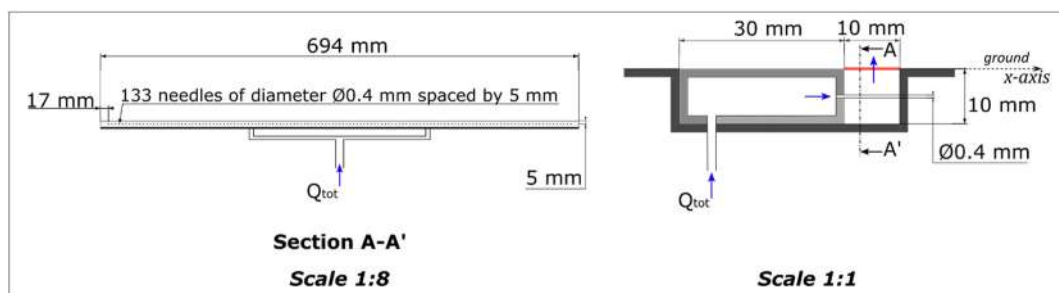


**Fig. 6.** Sketch of the detailed design of the pollutant source.

wind tunnel both along the source and at varying distances from it. In Marro et al. [76], the homogeneity of the scalar release, using the same source, was confirmed through a mass balance between the mass flow per unit length released at the source (at a specific y-coordinate) and the longitudinal evolution of the mass flow integrated over the vertical axis at the same y-coordinate. Furthermore, in the recent work of Fellini et al. [15], the same emitting source was installed in a longer street (1 m long) and a symmetric concentration field was observed inside the street canyon. From these studies, the homogenous emission was verified for different lengths of the same source. On the other hand, previous experiments conducted in the same wind tunnel revealed that it is more difficult to obtain a perfectly symmetric flow and concentration field in a shorter street canyon, as discussed further in Section 4.

2.3.2. Concentration measurement

Concentration measurements were performed with the HFR400 Fast FID is commonly used for measuring the concentration field in geometries resembling urban canyons [15,78,79]. The instrument was equipped with a long sampling capillary tube 30 cm in length and supported with a metal brace of 2.5 mm thickness, allowing a frequency response of 400 Hz [57]. The tube, with a radius of  $1.27 \times 10^{-4}$  m, was mounted on its head and positioned above the test section to avoid affecting the flow field. The pressure drop imposed along the capillary tube was 33330.6 Pa (Pa). The instrument can detect concentration values

between 0 and 5000 parts per million (ppm) in the range of 0–10 V with an accuracy of about 1–2 ppm. The calibration was carried out using ethane–air mixtures with concentrations equal to 0, 500, 1000, and 5000 ppm. Generally, calibration was performed twice a day. When the flame temperature showed variations of more than 2 °C from the value recorded at the beginning of the experiment, calibration was repeated. A more detailed description of the FID is provided by Marro et al. [76]. The measurement error of the concentration was found to be 3 %, as noted in other studies which used the same FID for their experimental setup [57, 76,80].

All measurements were performed in statistically steady conditions: a mixture of air and ethane was injected at a constant flow rate from the ground level source. At each point, a sampling time of 2 min (min) was adopted, which provides a reliable estimate of the mean concentration. Moreover, before and after each acquisition, the background concentration was recorded by stopping the emission for 15 s (s) (allowing for the transients to settle). The background concentration, which was assumed to evolve linearly with time from its initial to its final value, was then subtracted from the signal [15,76,80]. The concentration within the cavity was measured at around 200 sampling points for each configuration scenario investigated. The measurement grid was defined to characterise the entire three-dimensional volume in detail and to better investigate the influence of obstacles on source-receptor relationships. The sketches showing the measurement points relative to

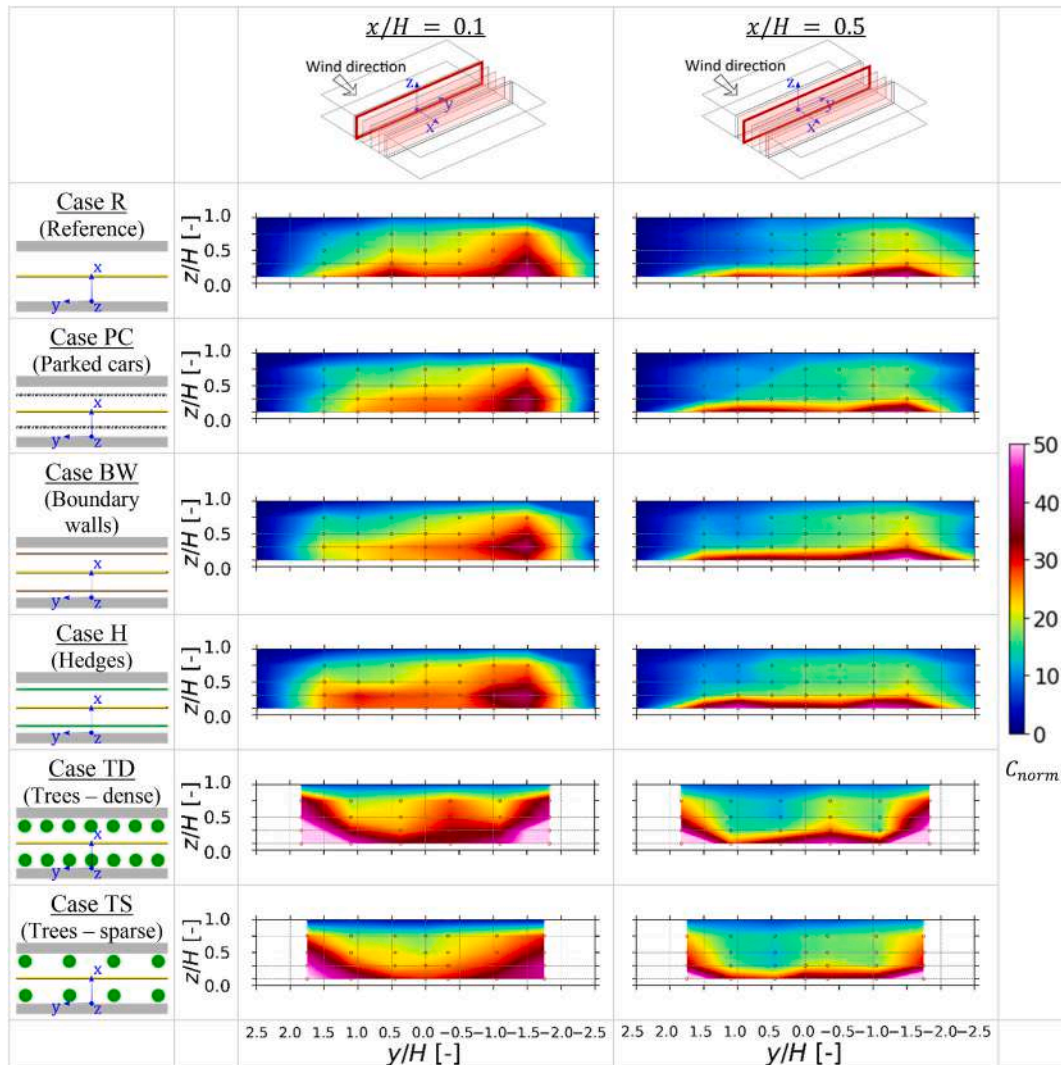


Fig. 7. Concentration fields shown for each case scenario, with planes being normal to the x-axis.

each obstacle have been provided in Appendix A (supplementary material). In the following, the non-dimensional concentration results are expressed as  $C_{norm} = CU_{\infty}L_sH/Q_{eth}$ , where  $C_{norm}$  is the time-averaged concentration of ethane at each sampling point,  $L_s$  is the source length, and  $Q_{eth}$  is the mass flow rate of ethane.

### 3. Results

#### 3.1. Concentration sections

The concentration field inside the urban canyon for each scenario is reported in Figs. 7–9, as 2-dimensional sections perpendicular to the x-axis, y-axis, and z-axis, respectively.

The images in Fig. 8 show that the pollutant accumulation as well as the changes in concentration levels in the presence of obstacles are most pronounced in the vicinity of the bottom-left corner, designating it as a region of greater concern. This is the breathing zone near the leeward (upwind) wall, and most of the following discussions would be focused on this zone. Consequently, Figs. 7 and 9 exclusively show the section images closer to the leeward wall ( $x/H = 0.1$  and  $x/H = 0.5$ ) and ground level ( $z/H = 0.1$  and  $z/H = 0.3$ ), respectively. The figures showing the concentration field for the other sections, as well as the standard deviation of concentration field for all the sections, are provided in Appendix A.

Fig. 7 shows that the concentration levels drop to zero at the top and lateral edge of the canyon for all the cases, showing efficient ventilation

in these regions. The left panels in Fig. 7 also suggest that a higher concentration of pollutants accumulates on the leeward façade, posing a hazard for residents living in these spaces with open windows. For parked cars, boundary walls and hedges, the change in concentration levels with respect to the reference case appears to be negligible, while dense and sparse trees show higher concentration levels. The increase in concentration in the presence of trees is possibly due to the lower ventilation levels and the ‘trapping’ effect cited by earlier research (see Section 1).

Fig. 8 shows that, regardless of the presence of obstacles, there is a clear increase in the pollutant concentration near the leeward (upwind) wall than the windward (downwind) wall. Fresh air enters the canyon near the roof of the windward wall and the lateral ends, and transports the pollutant released from the centre of the canyon towards the leeward wall. Most of the pollutant is hence accumulated along the leeward wall, while a smaller portion is diffused/recirculated towards the windward wall.

Comparing the left and right panels in Fig. 9, the left panels show the highest accumulation of pollutant concentration in the lowest part of the street canyon, close to the pedestrian level. The lowest level of measurement is done at  $z/H = 0.1$ , corresponding to 2 m above ground level (for a 1:200 scale), and is relatively close to the pedestrian breathing height (usually taken at 1.5 m above ground level). Moreover, in this pedestrian zone, the concentration increase is neither symmetric about the centre  $y/H = 0$  (as seen for Cases R, PC, BW and H), nor homogenous (as seen for Case TD and TS) as concentration peaks observed off-centre.

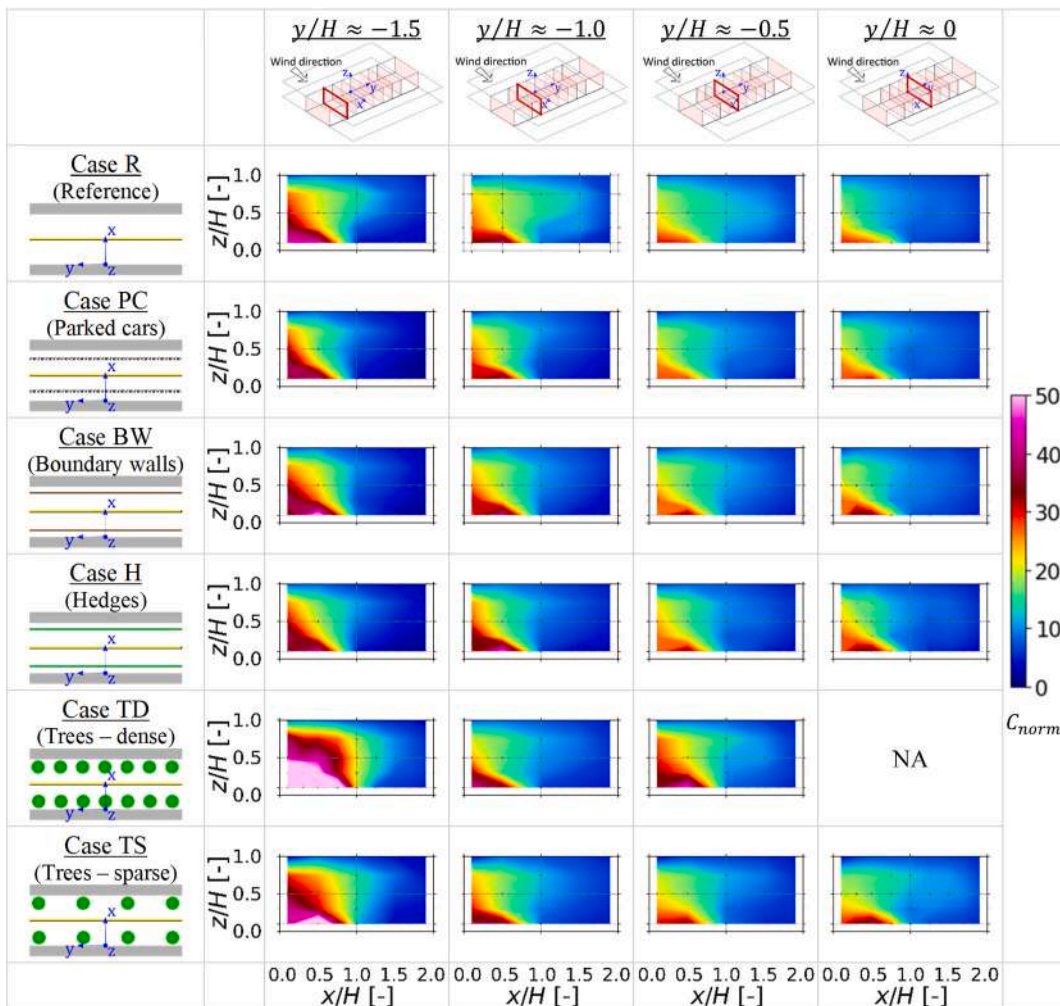


Fig. 8. Concentration fields shown for each case scenario, with planes being normal to the y-axis.

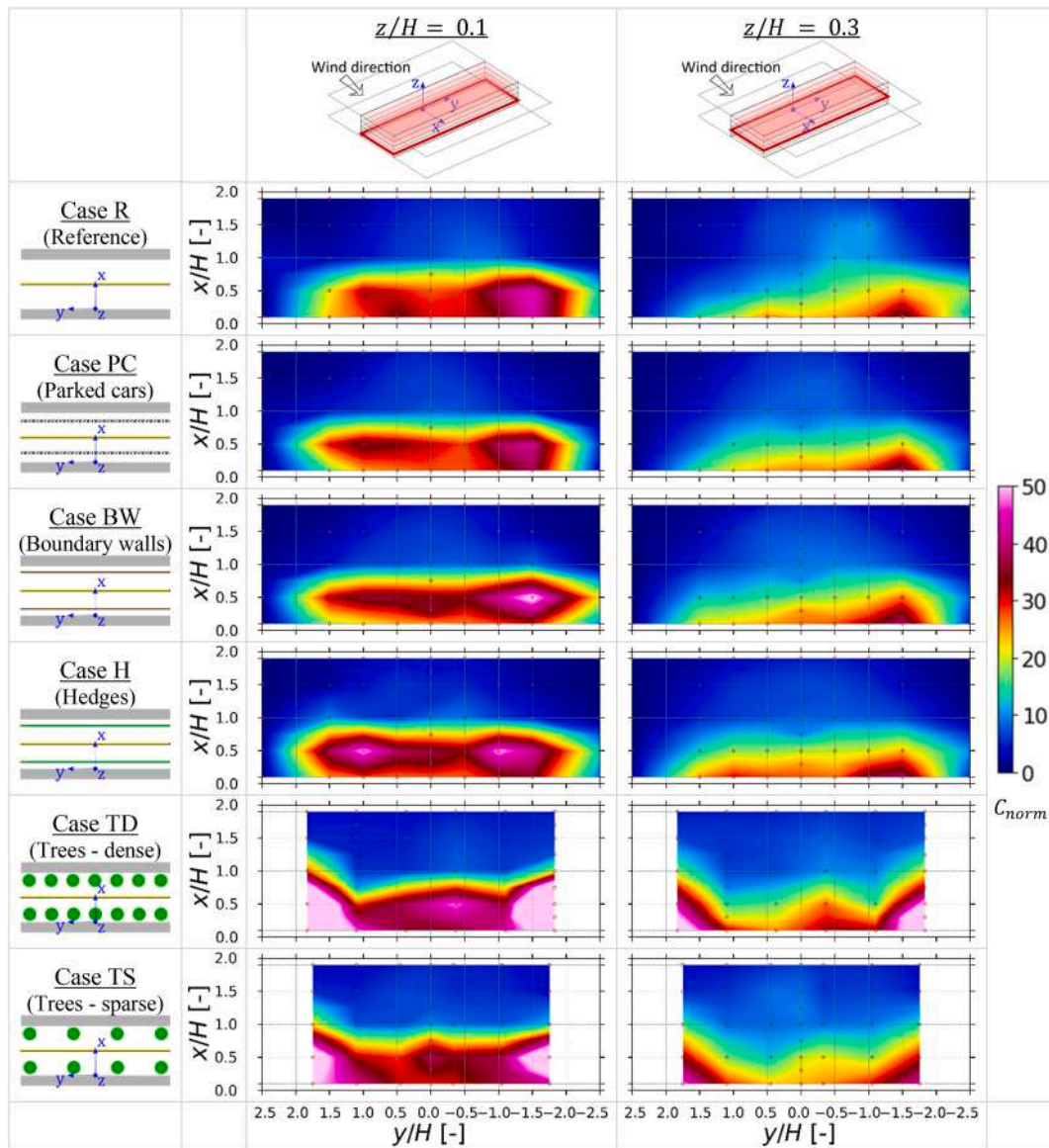


Fig. 9. Concentration fields shown for each case scenario, with planes being normal to the  $z$ -axis.

The observed asymmetry is possibly due to experimental uncertainty. However, the inhomogeneity, observed as concentration peaks in the presence of trees, was also found in the experimental study conducted by Fellini et al. [15]. These features will be discussed in Section 4.

From Fig. 7, for parked cars, boundary walls and hedges, changes in the pollutant concentrations relative to the reference case are mostly observed closest to the obstacles. For instance, in the left-hand panel of Fig. 9 for  $z/H = 0.1$ , all three cases show a reduction in pollutant concentration at  $x/H = 0.1$  compared to the reference case. This is in line with other studies [26] highlighting that low-level obstacles along the pedestrian sidewalk can alter the dispersion pathways between the source and the receptor, thus changing the concentration levels in the breathing zone. The tangible reductions in concentration for this zone are discussed further in Section 4.

From Fig. 7, for dense and sparse tree cases, there is an increase in pollutant concentration compared to the reference case along the leeward wall. Again, higher concentrations are observed closest to the pedestrian zones. Dense trees show a marked increase compared to sparse trees, and in both these configurations the concentration at  $y/H = 1.75$  is higher than at  $y/H = 0$ .

### 3.2. Concentration profiles

The longitudinal profiles of concentration levels averaged over the  $z$ -axis are shown in Fig. 10. Only the concentration profiles along the leeward wall are shown and discussed here, while the results and concentration profiles of the other areas (closer to the centre and windward wall) are included in Appendix A. This is because, from Fig. 8, it is observed that the concentration along the leeward wall ( $x/H = 0.1$ ) is measurably more pronounced (approximately 5–10 times higher) than the concentration along the windward wall ( $x/H = 1.9$ ).

For some obstacles scenarios, the concentration values were measured at the end of the street canyon (at  $y/H = \pm 2.5$ ), while the FID measurement process was impeded by the presence of the trees. Moreover, any concentration results obtained there are negligible due to the transport of pollutants away from the street canyon by direct influence from the lateral wind flow. Hence, the measured values at these points have been removed from calculations henceforth.

Since the concentration profiles are averaged along the  $z$ -axis, Fig. 10 does not distinctly show the variations in concentration at the pedestrian level. This is where obstacles like parked cars, boundary walls and hedges are most likely to influence the dispersion pattern. The left panel

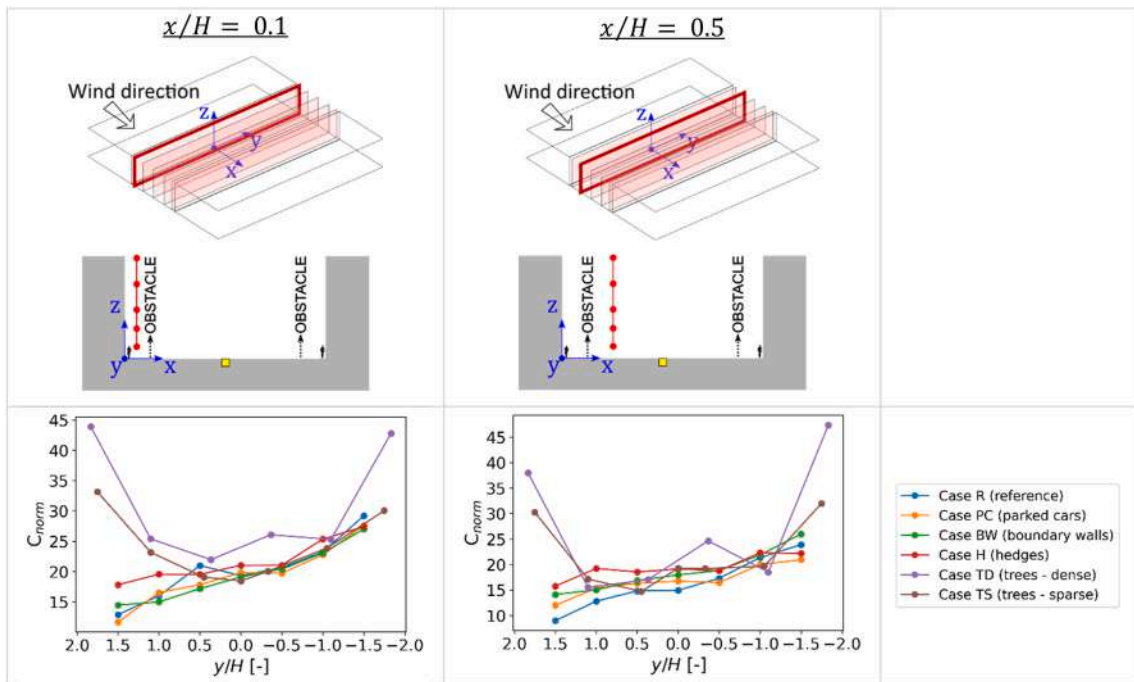


Fig. 10. Concentration profiles (bottom row) plotted along the y-axis for fixed  $x/H$ . Each measured point is averaged along the z-axis. Top row contains sketches indicating the measurement position in red. (For interpretation of the references to colour in this figure legend, the reader is referred to the Web version of this article.)

of Fig. 10 ( $x/H = 0.1$ ) shows minimal perceptible differences between these obstacles (i.e., parked cars, boundary walls and hedges), while the right panel ( $x/H = 0.5$ ) shows a slight increase for the same cases, hinting that these obstacles obstruct the pollution coming from the street. To better illustrate this difference in concentration patterns at the pedestrian height, the concentration profiles in this zone are shown in

Fig. 11, especially near the leeward wall for the reasons clarified earlier. Comparing Fig. 10 with Fig. 11, it is evident that parked cars, boundary walls and hedges have minimal effect on pollutant dispersion when the concentration is averaged along the z-axis (Fig. 10), but there is a sizeable impact in the region near these obstacles (as depicted in Fig. 11), specifically in the breathing zone (i.e., at  $z/H = 0.1$ ). The left

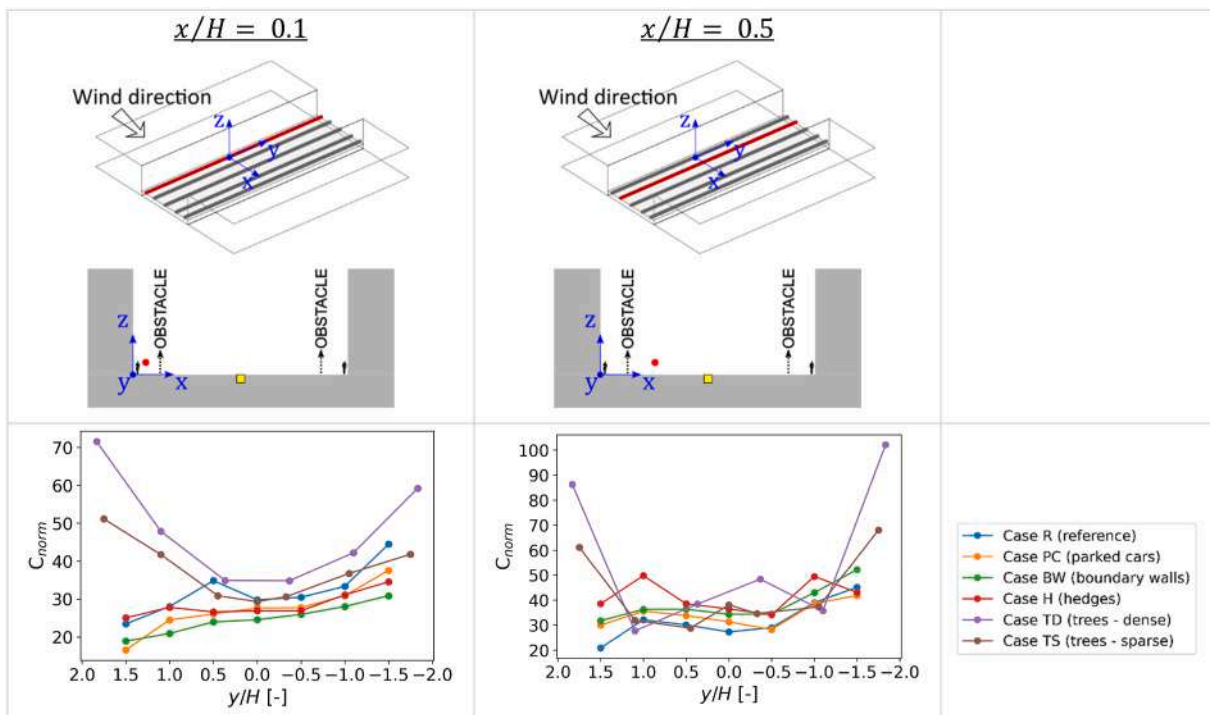


Fig. 11. Concentration profiles (bottom row) plotted linear to the y-axis for fixed  $x/H$ . Each measured point is obtained at the pedestrian breathing zone height of  $z/H = 0.1$ . Top row contains sketches indicating the measurement position in red. (For interpretation of the references to colour in this figure legend, the reader is referred to the Web version of this article.)

panels in Fig. 11 for parked cars, boundary walls and hedges show reduced concentration along the leeward pedestrian wall (at  $x/H = 0.1$ ). Conversely, these obstacles seem to cause an increased concentration along the leeward roadway (at  $x/H = 0.5$ ), restricting the pollution to the roadway itself.

### 3.3. Zones of interest

Based on the results seen in Fig. 11, five primary zones of interest can be identified as follows (with a reference image shown in Fig. 12).

1. Leeward pedestrian zone (Line 1) – The region between  $x/H = 0$  to  $x/H = 0.2$ . Measured by the concentration values taken at  $x/H = 0.1$  and  $z/H = 0.1$ .
2. Leeward street zone (Line 2) – The region between  $x/H = 0.3$  to  $x/H = 0.7$ . Measured by the concentration values taken at  $x/H = 0.5$  and  $z/H = 0.1$ .
3. Central zone (Line 3) – The region between  $x/H = 0.7$  to  $x/H = 1.3$ . Measured by the concentration values taken at  $x/H = 1.0$  and  $z/H = 0.1$ .
4. Windward street zone (Line 4) – The region between  $x/H = 1.3$  to  $x/H = 1.7$ . Measured by the concentration values taken at  $x/H = 1.5$  and  $z/H = 0.1$ .
5. Windward pedestrian zone (Line 5) – The region between  $x/H = 1.8$  to  $x/H = 2.0$ . Measured by the concentration values taken at  $x/H = 1.9$  and  $z/H = 0.1$ .

Since low-level obstacles like cars, hedges and boundary walls significantly influence the source-receptor relationship at the breathing zone height (see Section 1), investigating these regions would yield the most significant findings from this experimental study.

Line 1 in Fig. 11 (left panel), for parked cars, boundary walls and hedges, shows that the concentration values along the pedestrian sidewalk are slightly lower compared to the reference case. However, along Line 2 in Fig. 11 (right panel), which is on the roadway, the concentration values are higher. This shows that these obstacles do alter the flow of pollutants to the benefit of pedestrians. However, the distribution of the concentration is slightly asymmetric along the length of the canyon for these scenarios, including the reference case, as the concentration leans more towards one of the lateral ends of the canyon ( $y/H = -1.5$ ) than the other. This asymmetry is discussed further in Section 4.

Line 1 and Line 2 in Fig. 11, for dense and sparse trees, show the concentration values appear higher in comparison with the reference case. The spread of the concentration is also quite inhomogeneous, as

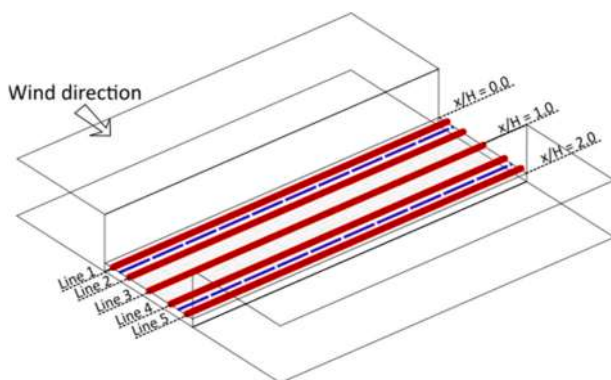


**Fig. 12.** Reference image showing the five primary regions of interest in red lines; Line 1 is along the leeward wall with the highest concentration levels, while Line 5 is along the windward wall. The blue semi-dotted line represents the approximate position of the obstacles. (For interpretation of the references to colour in this figure legend, the reader is referred to the Web version of this article.)

the pollutant appears to peak at  $y/H = \pm 1.75$ . This peaked concentration is also discussed further in Section 4.

### 3.4. Average distribution in zones of interest

To better investigate and summarise the effect of obstacles on pollutant concentration along each of the zones depicted in Fig. 12, we average the concentration values for each. In Fig. 13, these averaged values are compared against the reference case as a percentage improvement, i.e., a percentage decrease in pollutant concentration.

For Line 1 in Fig. 13, parked cars, boundary walls and hedges show an improvement in air quality compared to the reference case (a decrease in pollutant concentration of 15 %, 23 % and 11 % respectively). On the other hand, dense and sparse trees show a deterioration in pollutant concentration levels (an increase in pollutant concentration of  $-51$  % and  $-17$  % respectively). A similar pattern can be observed along Line 5 (the windward side).

From Line 2 in Fig. 13, dense and sparse trees continue to show a deterioration in concentration levels, with an increase in pollutant concentration of 77 % and 34 % respectively. But also parked cars, boundary walls and hedges show a worsening of the air quality compared to the reference case (with an increase in pollution levels of 7 %, 20 % and 32 %). This may be associated with the pollutant impediment characteristic of these obstacles, also mentioned as the 'blocking effect' in previous literature [81–83].

Along Line 3 in Fig. 13, which is the centre of the street canyon, every obstacle scenario shows a deterioration in pollutant concentration levels. Dense and sparse trees show the highest deterioration compared to the reference case, with concentration increments of 104 % and 75 % respectively.

Along Line 4 and Line 5 in Fig. 13, parked cars, boundary walls and hedges show an improvement in pollutant concentration levels over reference case, compared to dense and sparse trees which show a deterioration of air quality. We note that the absolute concentration levels are considerably lower here than on the leeward side wall (refer to Fig. 8), so this region is much less hazardous in general.

### 3.5. Pedestrian zone surface level average comparison

Fig. 14 show the surface level average comparison of the pollution concentration across the entire street canyon at the pedestrian breathing zone height. This serves to understand the overall influence of each obstacle.

From Fig. 14, non-porous obstacles such as parked cars and boundary walls both show an improvement in air quality, given by a decrease in pollutant concentration of 4.5 % and 1.2 % respectively compared to the reference case for the entire breathing zone. On the other hand, porous obstacles such as hedges, dense trees and sparse trees show a worsening in concentration levels, with an increase of pollution levels of 7.3 %, 62.2 % and 28.6 % respectively.

### 3.6. Canyon volume average comparison

Finally, we present in Fig. 15 the volume average comparison of the pollution concentration for the entire street canyon.

From Fig. 15, only the parked cars show an improvement in overall air quality in the urban canyon given by a decrease in pollutant concentration of 4.8 %, while boundary walls show an almost negligible worsening of 0.7 %. Porous obstacles such as hedges, dense trees and sparse trees show a worsening in concentration levels, with an increase of pollution levels of 5.6 %, 70.5 % and 22.3 % respectively.

## 4. Discussion

In this section, we will delve into specific aspects of the concentration distribution within the canyon, as revealed by the results presented

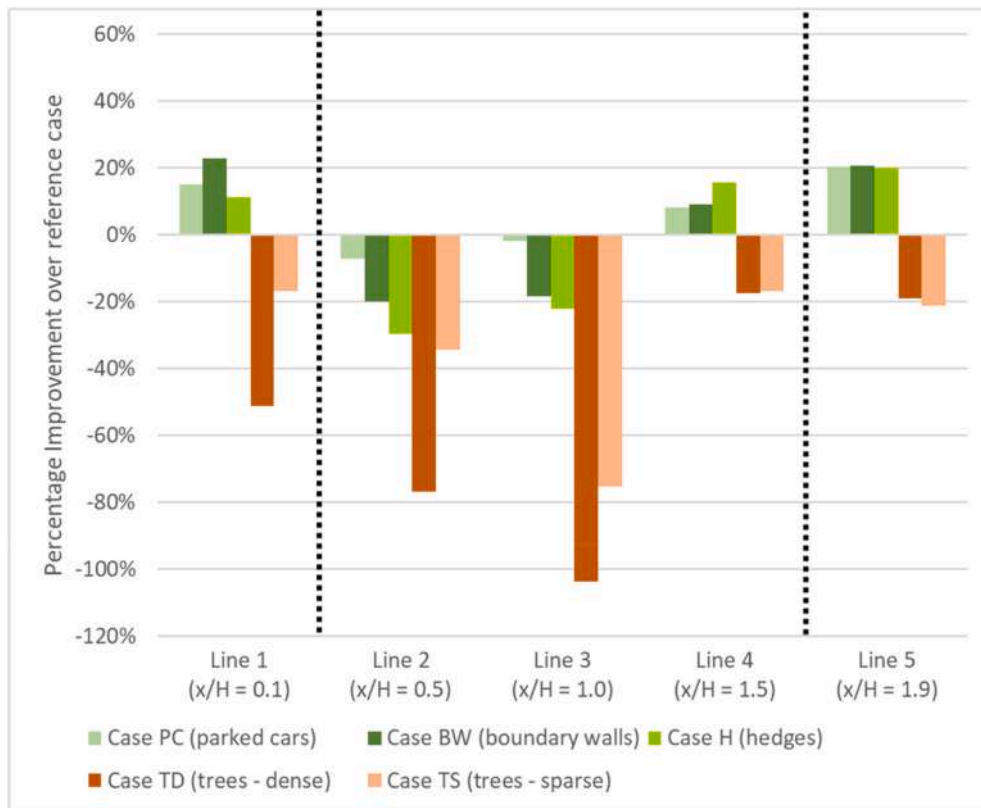


Fig. 13. Averaged concentration values for each obstacle case compared against the reference case, represented as a percentage improvement. Results are averaged between each lateral end ( $y/H = -2.5$  to  $+2.5$ ) and for the breathing zone height at  $z/H = 0.1$  (see Fig. 12). Dotted black line indicates the relative position of the obstacles.

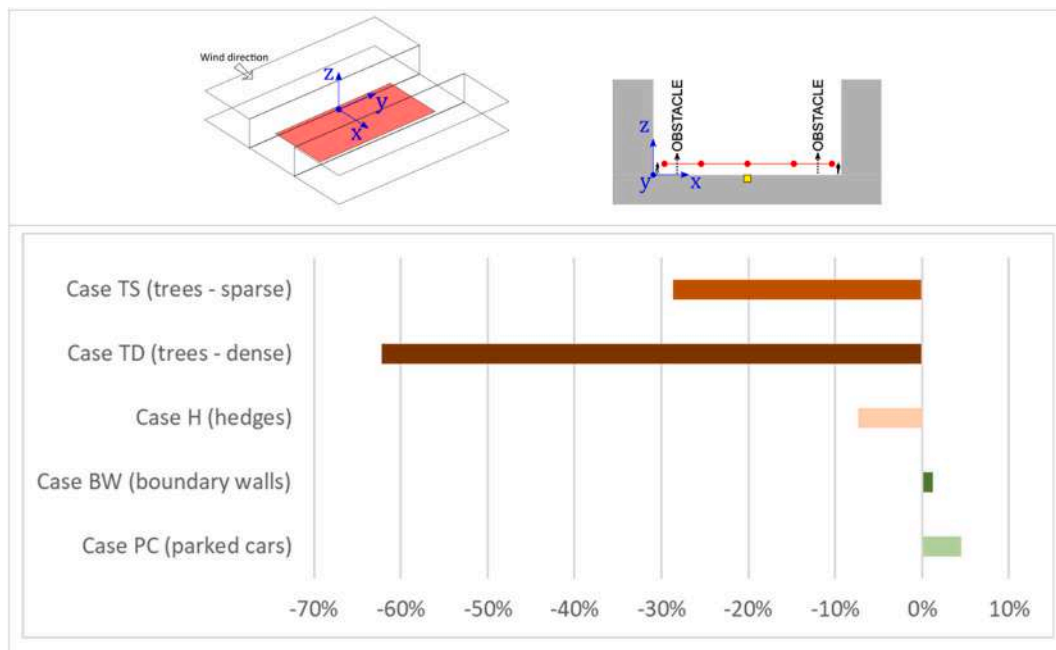
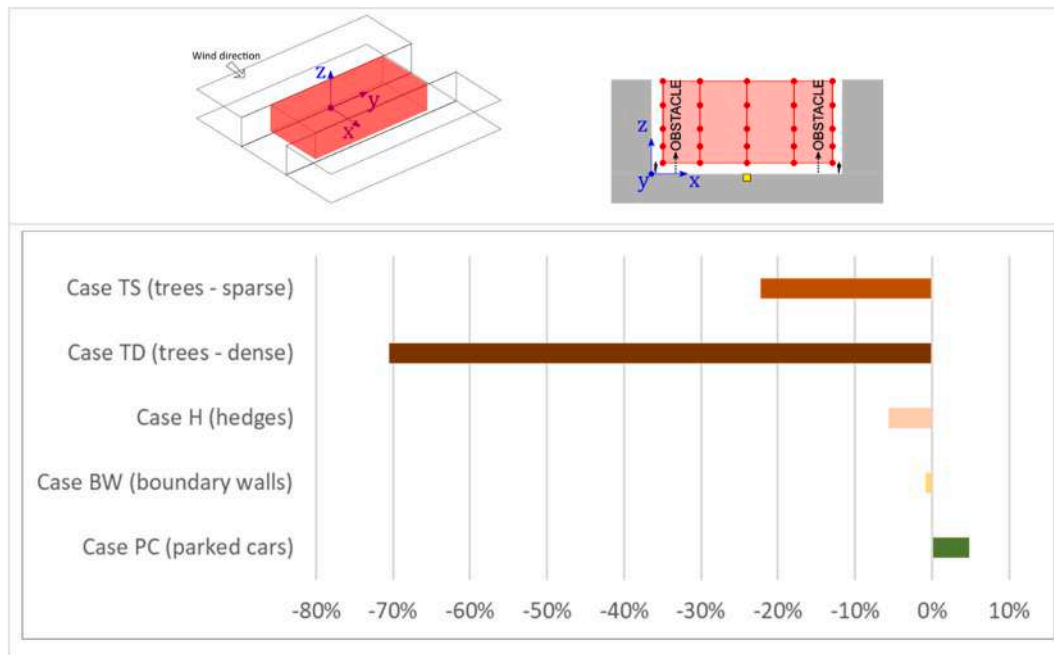


Fig. 14. Surface level average comparison of the concentration values obtained for the pedestrian height zone (red area shown in sketch above), for each obstacle case compared against the reference case. (For interpretation of the references to colour in this figure legend, the reader is referred to the Web version of this article.)

in the preceding sections.

The accumulation of pollutants towards the leeward wall as seen in Fig. 8 possibly suggests the formation of a primary vortex development within the canyon, indicative of either a skimming or wake interference

flow regime [84]. For canyon  $H/W$  ratio equal to 0.5 with  $L/W$  ratio equal to 5, a skimming flow regime would be contrary to Oke's study [84], which expects the flow regime to be a wake-interference flow when  $H/W$  ratio is less than 0.65. However, the numerical study by



**Fig. 15.** Volume average comparison of the concentration values obtained for the pedestrian height zone (red volume shown in sketch above), for each obstacle case compared against the reference case. (For interpretation of the references to colour in this figure legend, the reader is referred to the Web version of this article.)

Hunter et al. [85] observed a transition to wake interference flow for canyon  $H/W$  ratio equal to 0.5, while the field study by Johnson and Hunter [86] observed a skimming flow pattern even for  $H/W$  ratio equal to 0.4. These studies support the claim by Oke [84], that building geometrical ratios are not strictly indicative of the flow regime within the canyon. Hence either a skimming or wake interference flow regime is speculated for this study from the pollutant accumulation profiles seen along the leeward wall.

The asymmetry highlighted in the previous section, seen from the higher distribution of concentration towards one of the lateral ends ( $y/H = -1.5$ ) in the reference case (see Fig. 9) can be attributed to experimental factors. As already pointed out in previous studies performed in this experimental facility, the flow developing within the WT, even in the absence of obstacles placed on the floor, is not always parallel to the WT axis. Indeed, as widely discussed by Nironi et al. [57] and Marro et al. [87,88] the trajectory of the centre of mass of a scalar plume emitted from an elevated point source is slightly deflected by an angle of  $2.5^\circ$  when travelling downstream. The study by Fuka et al. [89] comparing CFD with WT results also commented on the difficulty of obtaining a perfectly symmetric condition in a WT by a scalar pollutant source emitted for a multiple canyon configuration. Similar asymmetries can be observed in other studies when analysing the passive scalar dispersion within a densely packed regularly spaced array of buildings [60,90]. These studies also show that the flow within the array becomes increasingly sensitive to tiny errors in the arrangement of the blocks as the width of the lateral streets (whose axis is perpendicular to the direction of external flow) increases, i.e., as the height-to-width ( $H/W$ ) ratio is below unity. In this case, the geometry of the intersection tends to amplify flow instabilities caused by slight asymmetries in the obstacle array, resulting in an asymmetric pollution concentration pattern [91, 92]. The presence of the intersection on either lateral side causes the formation of double eddy circulation patterns (corner vortices) with a vertical axis entraining fresh air from the lateral shear layer [93,94], and minor differences in the flow speeds on each of the lateral ends can alter the wind flow ingress differently, causing an asymmetry of the pollutant dispersion within the canyon [91,95,96].

Another interesting result is the peaked concentration at  $y/H = \pm 1.75$ , observed for dense and sparse tree cases in Fig. 9. This pattern has

been previously addressed in the literature [15,25], where it was highlighted that the presence of trees alters the flow dynamics within the street, leading to a distinct spatial organisation of the concentration field within the canyon. This suggests that large obstacles like trees impact the formation of canyon vortices and corner eddies differently. This distinction is crucial for two reasons: first, Li et al. [93] noted how lateral entrainment induced by corner eddies might lead to a more significant reduction in pollutant concentrations within an urban canyon, but second, lateral entrainment would have an adverse effect on a larger urban scale, transporting pollutants further windward while keeping them within the urban canopy, potentially increasing the mean age of air and worsening city breathability within the urban canyon layer [97]. Therefore, lateral entrainment is less favourable, compared to top entrainment (from the roof level) which enhances the dilution rate, i.e., the outward flux of pollutants that never returns. The observation of concentration peaking in the presence of large trees (Cases TD and TS), not evident in the case of other obstacles (Cases PC, BW, H), suggests that large trees may substantially weaken corner eddies responsible for lateral entrainment while having a much milder effect on the central canyon vortex responsible for top entrainment. The region of the pedestrian breathing zone where this peaking occurs can be referred to as “pollution hotspots”. To prove this phenomenon better, further investigative studies are needed, as they could significantly support the endorsement of trees in urban canyons. If appropriately installed, like shown in the study by Abhijith and Gokhale [33] for a combination of high porosity trees and parked cars, trees could offer relief to pedestrians along sidewalks, reduce lateral entrainment, and enhance top entrainment all at once.

To discuss the average concentration distribution in the zones of interest shown in Fig. 13 in Section 3.4, it is seen that for zones designated as pedestrian sidewalks along Line 1 and Line 5, parked cars, boundary walls and hedges tend to impede the pollutants coming from the roadside thus reducing concentration exposure for pedestrians. On the other hand, trees appear to trap and increase concentration levels. It is unclear if this trapping effect is due predominantly to the loss of momentum in the wind flow, or also because of increasing turbulence dissipation caused by the trees in this specific street canyon configuration [32,37], but more investigative studies would be required.

The effect of street trees on pollutant dispersion is complex. Stand density, canopy, arrangement, crown height, leaf deposition, etc, are just a few of the many variables that would affect the quality of the air within the canyon [98]. Case in point, when accounting for the change in the linear stand density between dense and sparse trees, halving the linear stand density of the trees reduces the average deterioration in concentration level by two-thirds along the pedestrian sidewalk (from  $-51\%$  in Case TD to  $-17\%$  in Case TS). Thus, altering few of the vegetation variables such as porosity or crown size could offset the trapping effect, leading to improvements in concentration levels along the pedestrian sidewalk.

The results presented in Section 3.1 also provide valuable insights for discussing the practical implications of this study. The area along the windward side, but still within the roadway, observed by Line 4 from Fig. 12, shows relatively lower pollution concentrations than the leeward side. This region could be suitable for bicycle lane design. Moreover, Line 4 in Fig. 13 indicates further improvement of concentration levels in the presence of obstacles like parked cars, boundary walls and hedges. This may be due to the changing vortex structures associated with the presence of obstacles (as highlighted in Section 1), and further research may be necessary to gain clarity on the flow dispersion dynamics in this area.

Another interesting matter of discussion is the effect of obstacle size and material properties. Line 1 in Fig. 13 indicates that the height of the barrier is an important factor. Parked cars and boundary walls are both non-porous obstacles, yet the taller boundary wall shows better improvement compared to parked cars ( $23\%$  vs  $15\%$  respectively). The relationship between obstacle height and the reduction of pollutant exposure has been recorded in previous studies (refer to Section 1). However, in a real street canyon, there may be limitations in how high a barrier could be installed.

The porosity and surface roughness of the obstacle also influence pollutant reduction in the pedestrian zone. For instance, when comparing only boundary walls with hedges from Fig. 13, both obstacles have the same geometrical size and position, differing instead in their porosity and surface roughness (boundary walls being non-porous and smooth, while hedges being porous and rough). Yet hedges show an increase in concentration along Line 2. This is probably due to the greater surface roughness of porous hedges that reduces the flow speed in this region, thus causing a slower dispersion of pollutants. In addition, one might anticipate that the concentration behind the hedges along Line 1 would be lower when compared with boundary walls given the blocking effect mentioned earlier. However, this is not the case. The porosity of the hedges allows pollutants to diffuse through the medium, potentially resulting in increased concentration levels along the pedestrian sidewalk on Line 1. Further corroboration can be found from Fig. 13 when comparing parked cars with hedges. Despite the parked cars being shorter than the hedges, they provide a higher reduction in pollutant concentration levels along Line 1 ( $15\%$  vs  $11\%$  respectively), indicating that obstacle porosity and/or surface roughness are important design considerations.

From the surface level average comparison shown in Fig. 14 in Section 3.5, the  $4.5\%$  efficacy of parked cars in Fig. 14 is notably higher than the  $1.2\%$  efficacy of boundary walls. Although the taller boundary wall yields better performance along Line 1 (the pedestrian sidewalk) as shown earlier, the worsening of concentration levels along Line 2 may offset these benefits. Citing the earlier referenced CFD study by Wang et al. [48] (see Section 1) which observed the influence of changing wind speed on the expansion/compression effect of the vortices and eddies generated in the canyon, it may be suggested that the barrier height of non-porous obstacles similarly influences the flow patterns and thus the pollutant distribution over the surface near the obstacles.

Hedges show a  $7.3\%$  worsening of air quality in Fig. 14. As porous media tends to have a trapping effect on pollutants (see Section 1), this may lead to an overall worsening of air quality in the region near hedges. Yet hedges demonstrate lower concentrations along Line 1 in Fig. 13

when compared with the reference case, thus ensuring it is still beneficial along the sidewalks.

From Fig. 14, dense and sparse trees show a  $62.2\%$  and  $28.6\%$  worsening of air quality at the surface level, which might be attributed to the canyon-wide trapping effect of trees [36,99,100] (see Section 1). Given that trees have various associated variables, any further quantitative assessment would be speculative. This study models only a gaseous pollutant, and porous obstacles differently influence particulate type pollutants. Furthermore, a combination of obstacles, such as hedges or boundary walls coupled with varying tree variables could potentially offer benefits for pedestrians as highlighted in earlier research [36,38].

To finalise with the discussions on the volume average comparison shown in Fig. 15, only parked cars show a definite improvement in air quality of  $4.8\%$ , followed by boundary walls that show a slight worsening of  $0.7\%$ . As discussed earlier, the case for barrier height effecting the pollutant distribution over the full canyon, especially in a laterally open canyon, should primarily influence the formation and strength of eddies at the lateral ends, and thus the overall ventilation efficiency within the canyon [93,94,101,102]. Meanwhile, the case for hedges, dense and sparse trees showing a worsening of  $5.6\%$ ,  $70.5\%$  and  $22.3\%$  in concentration levels may be attributed to the ‘trapping’ effect elucidated earlier. More detailed studies, utilising WT experiments and CFD simulations may yield more conclusive evidence, especially in isolating the variables that influence these concentration levels. Nonetheless, the canyon surface-level and volume averaged comparison for all cases, shown in Figs. 14 and 15 respectively, remains important from a CFD validation standpoint.

## 5. Conclusions

In accordance with the aims of this study, the evidence drawn from the results supports the claim that different obstacles and their geometrical parameters would have different effects on the pollutant concentrations at the pedestrian zone height.

Along the pedestrian sidewalk on both the leeward and windward wall side, parked cars, boundary walls and hedges all show improvement in air quality, with porosity, surface roughness and height of the obstacle acting as potential indicators of the dispersion performance of obstacles and requiring further investigative studies.

Dense and sparse trees show a deterioration in air quality, as well as the creation of pollution hotspots along the pedestrian sidewalks. However, this study comparatively investigated only the change in the linear stand density, while street trees have many other indicators that could alter the flow dispersion and pollutant concentrations within an urban canyon. Hence, it would be necessary to conduct more experimental and CFD simulations, especially in the context of real urban canyons, to ascertain which variables should be altered for the benefit of pedestrians.

True to the objectives of this paper, the assessment of these different obstacles suggests that the implementation of different types of obstacles would affect the pollutant dispersion within the street canyon and is an effective and low-cost method of abating the negative health effects to pedestrians. Exploring specific quantitative correlational patterns between the variables of different obstacles would be an interesting avenue for future research, and the experimental database presented herein serves as a valuable validation tool for practitioners and researchers hoping to investigate different scenarios of obstacles with CFD/numerical simulations.

## CRedit authorship contribution statement

**Oliver S. Carlo:** Writing – original draft, Visualization, Methodology, Investigation, Formal analysis. **Sofia Fellini:** Writing – review & editing, Visualization, Validation, Methodology. **Olga Palusci:** Writing – review & editing, Visualization, Methodology, Formal analysis. **Massimo Marro:** Writing – review & editing, Visualization, Validation,

Investigation. **Pietro Salizzoni**: Writing – review & editing, Validation, Resources, Project administration, Methodology. **Riccardo Buccolieri**: Writing – review & editing, Supervision, Methodology, Formal analysis, Conceptualization.

### Declaration of competing interest

The authors declare that they have no known competing financial interests or personal relationships that could have appeared to influence the work reported in this paper.

### Data availability

Data will be made available on request.

### Acknowledgements

Oliver S. Carlo acknowledges the financial support within the “Dipartimento di Eccellenza fundings” – Ph.D. XXXVI cycle – University of Salento. Sincere gratitude goes to all the anonymous reviewers for their expert comments and suggestions which have greatly contributed to the quality of this paper.

### Appendix A. Supplementary data

Supplementary data to this article can be found online at <https://doi.org/10.1016/j.buildenv.2023.111143>.

### References

- [1] OECD, OECD Environmental Outlook to 2050 : the Consequences of Inaction, 2012. <https://www.oecd.org/env/indicators-modelling-outlooks/oecdenvironmentaloutlookto2050theconsequencesofinaction-keyfactsandfigures.htm>.
- [2] S. Alam, A. Khan, The impact study of vehicular pollution on environment, *Int. J. Sci. Adv. Res. Technol.* 6 (2020) 30–37. [www.ijrsart.com](http://www.ijrsart.com).
- [3] C. He, K. Qiu, R. Pott, Reduction of traffic-related particulate matter by roadside plants: effect of traffic pressure and sampling height, *Int. J. Phytoremediation* 22 (2019) 1–17, <https://doi.org/10.1080/15226514.2019.1652565>.
- [4] X. Wang, M. Teng, C. Huang, Z. Zhou, X. Chen, Canopy density effects on particulate matter attenuation coefficients in street canyons during summer in the Wuhan metropolitan area, *Atmos. Environ.* 240 (2020) 117739, <https://doi.org/10.1016/j.atmosenv.2020.117739>.
- [5] Y. Huang, C. Lei, C.-H.H. Liu, P. Perez, H. Forehead, S. Kong, J.L. Zhou, A review of strategies for mitigating roadside air pollution in urban street canyons, *Environ. Pollut.* 280 (2021) 116971, <https://doi.org/10.1016/j.envpol.2021.116971>.
- [6] D. Voordeckers, T. Lauriks, S. Denys, P. Billen, T. Tytgat, M. Van Acker, Guidelines for passive control of traffic-related air pollution in street canyons: an overview for urban planning, *Landsc. Urban Plann.* 207 (2021) 103980, <https://doi.org/10.1016/j.landurbplan.2020.103980>.
- [7] Z. Li, T. Ming, S. Liu, C. Peng, R. De Richter, W. Li, Review on pollutant dispersion in urban areas-part A : effects of mechanical factors and urban morphology, *Build. Environ.* 190 (2021) 107534, <https://doi.org/10.1016/j.buildenv.2020.107534>.
- [8] Z. Li, T. Ming, T. Shi, H. Zhang, C.-Y. Wen, X. Lu, X. Dong, Y. Wu, R. de Richter, W. Li, C. Peng, Review on pollutant dispersion in urban areas-part B: local mitigation strategies, optimization framework, and evaluation theory, *Build. Environ.* 198 (2021) 107890, <https://doi.org/10.1016/j.buildenv.2021.107890>.
- [9] J. Gallagher, R. Baldauf, C.H. Fuller, P. Kumar, L.W. Gill, A. McNabola, Passive methods for improving air quality in the built environment: a review of porous and solid barriers, *Atmos. Environ.* 120 (2015) 61–70, <https://doi.org/10.1016/j.atmosenv.2015.08.075>.
- [10] R. Buccolieri, O.S. Carlo, E. Rivas, J.L. Santiago, P. Salizzoni, M.S. Siddiqui, Obstacles influence on existing urban canyon ventilation and air pollutant concentration: a review of potential measures, *Build. Environ.* 214 (2022) 108905, <https://doi.org/10.1016/j.buildenv.2022.108905>.
- [11] K.V. Abhijith, P. Kumar, J. Gallagher, A. McNabola, R. Baldauf, F. Pilla, B. Broderick, S. Di Sabatino, B. Pulvirenti, S. Di Sabatino, B. Pulvirenti, S. Di Sabatino, B. Pulvirenti, Air pollution abatement performances of green infrastructure in open road and built-up street canyon environments – a review, *Atmos. Environ.* 162 (2017) 71–86, <https://doi.org/10.1016/j.atmosenv.2017.05.014>.
- [12] P. Kumar, A. Druckman, J. Gallagher, B. Gatersleben, S. Allison, T.S. Eisenman, U. Hoang, S. Hama, A. Tiwari, A. Sharma, K. V. Abhijith, D. Adlakh, A. McNabola, T. Astell-burt, X. Feng, A.C. Skeldon, S. De Lusignan, L. Morawska, The nexus between air pollution, green infrastructure and human health, *Environ. Int.* 133 (2019) 105181, <https://doi.org/10.1016/j.envint.2019.105181>.
- [13] Y. Zhang, Z. Gu, C.W. Yu, Impact factors on airflow and pollutant dispersion in urban street canyons and comprehensive simulations: a review, *Curr. Pollut. Reports.* 6 (2020) 425–439, <https://doi.org/10.1007/s40726-020-00166-0>.
- [14] X.B. Li, Q.C. Lu, S.J. Lu, H. Di He, Z.R. Peng, Y. Gao, Z.Y. Wang, The impacts of roadside vegetation barriers on the dispersion of gaseous traffic pollution in urban street canyons, *Urban For. Urban Green.* 17 (2016) 80–91, <https://doi.org/10.1016/j.ufug.2016.03.006>.
- [15] S. Fellini, M. Marro, A.V. Del Ponte, M. Barulli, L. Soulhac, L. Ridolfi, P. Salizzoni, High resolution wind-tunnel investigation about the effect of street trees on pollutant concentration and street canyon ventilation, *Build. Environ.* 226 (2022) 109763, <https://doi.org/10.1016/j.buildenv.2022.109763>.
- [16] D. Sun, X. Shi, Y. Zhang, L. Zhang, Spatiotemporal distribution of traffic emission based on wind tunnel experiment and computational fluid dynamics (CFD) simulation, *J. Clean. Prod.* 282 (2021) 124495, <https://doi.org/10.1016/j.jclepro.2020.124495>.
- [17] J. Richmond-Bryant, M.G. Snyder, R.C. Owen, S. Kimbrough, Factors associated with NO<sub>2</sub> and NO<sub>x</sub> concentration gradients near a highway, *Atmos. Environ.* 174 (2018) 214–226, <https://doi.org/10.1016/j.atmosenv.2017.11.026>.
- [18] R. Ramponi, B. Blocken, L.B. de Co, W.D. Janssen, CFD simulation of outdoor ventilation of generic urban configurations with different urban densities and equal and unequal street widths, *Build. Environ.* 92 (2015) 152–166, <https://doi.org/10.1016/j.buildenv.2015.04.018>.
- [19] Y. Zhao, L.W. Chew, A. Kubilay, J. Carmeliet, Isothermal and non-isothermal flow in street canyons: a review from theoretical, experimental and numerical perspectives, *Build. Environ.* 184 (2020) 107163, <https://doi.org/10.1016/j.buildenv.2020.107163>.
- [20] P.J. Richards, S.E. Norris, Appropriate boundary conditions for computational wind engineering: still an issue after 25 years, *J. Wind Eng. Ind. Aerod.* 190 (2019) 245–255, <https://doi.org/10.1016/j.jweia.2019.05.012>.
- [21] M. Schatzmann, B. Leitl, Issues with validation of urban flow and dispersion CFD models, *J. Wind Eng. Ind. Aerod.* 99 (2011) 169–186, <https://doi.org/10.1016/j.jweia.2011.01.005>.
- [22] M. Schatzmann, S. Rafailidis, M. Pavageau, Some remarks on the validation of small-scale dispersion models with field and laboratory data, *J. Wind Eng. Ind. Aerod.* 67–68 (1997) 885–893, [https://doi.org/10.1016/S0167-6105\(97\)00126-8](https://doi.org/10.1016/S0167-6105(97)00126-8).
- [23] D.K. Heist, S.G. Perry, L.A. Brixey, A wind tunnel study of the effect of roadway configurations on the dispersion of traffic-related pollution, *Atmos. Environ.* 43 (2009) 5101–5111, <https://doi.org/10.1016/j.atmosenv.2009.06.034>.
- [24] C. Gromke, R. Buccolieri, S. Di Sabatino, B. Ruck, Dispersion study in a street canyon with tree planting by means of wind tunnel and numerical investigations - evaluation of CFD data with experimental data, *Atmos. Environ.* 42 (2008) 8640–8650, <https://doi.org/10.1016/j.atmosenv.2008.08.019>.
- [25] C. Gromke, B. Ruck, Influence of trees on the dispersion of pollutants in an urban street canyon-Experimental investigation of the flow and concentration field, *Atmos. Environ.* 41 (2007) 3287–3302, <https://doi.org/10.1016/j.atmosenv.2006.12.043>.
- [26] J. Gallagher, C. Lago, How parked cars affect pollutant dispersion at street level in an urban street canyon? A CFD modelling exercise assessing geometrical detailing and pollutant decay rates, *Sci. Total Environ.* 651 (2019) 2410–2418, <https://doi.org/10.1016/j.scitotenv.2018.10.135>.
- [27] J. Gallagher, L.W. Gill, A. McNabola, Optimizing the use of on-street car parking system as a passive control of air pollution exposure in street canyons by large eddy simulation, *Atmos. Environ.* 45 (2011) 1684–1694, <https://doi.org/10.1016/j.atmosenv.2010.12.059>.
- [28] J. Gallagher, L.W. Gill, A. McNabola, The passive control of air pollution exposure in Dublin, Ireland: a combined measurement and modelling case study, *Sci. Total Environ.* (2013) 458–460, <https://doi.org/10.1016/j.scitotenv.2013.03.079>, 331–343.
- [29] M. Ghasemian, S. Amini, M. Princevac, The influence of roadside solid and vegetation barriers on near-road air quality, *Atmos. Environ.* 170 (2017) 108–117, <https://doi.org/10.1016/j.atmosenv.2017.09.028>.
- [30] C. Gromke, A vegetation modeling concept for building and environmental aerodynamics wind tunnel tests and its application in pollutant dispersion studies, *Environ. Pollut.* 159 (2011) 2094–2099, <https://doi.org/10.1016/j.envpol.2010.11.012>.
- [31] R. Buccolieri, C. Gromke, S. Di Sabatino, B. Ruck, Aerodynamic effects of trees on pollutant concentration in street canyons, *Sci. Total Environ.* 407 (2009) 5247–5256, <https://doi.org/10.1016/j.scitotenv.2009.06.016>.
- [32] R. Buccolieri, J.L. Santiago, E. Rivas, B. Sanchez, B. Sánchez, B. Sanchez, Reprint of: review on urban tree modelling in CFD simulations: aerodynamic, deposition and thermal effects, *Urban For. Urban Green.* 31 (2019) 56–64, <https://doi.org/10.1016/j.ufug.2018.07.004>.
- [33] K. V. Abhijith, S. Gokhale, Passive control potentials of trees and on-street parked cars in reduction of air pollution exposure in urban street canyons, *Environ. Pollut.* 204 (2015) 99–108, <https://doi.org/10.1016/j.envpol.2015.04.013>.
- [34] C. Gromke, B. Ruck, Pollutant concentrations in street canyons of different aspect ratio with avenues of trees for various wind directions, *Boundary-Layer Meteorol.* 144 (2012) 41–64, <https://doi.org/10.1007/s10546-012-9703-z>.
- [35] A. Jeanjean, R. Buccolieri, J. Eddy, P. Monks, R. Leigh, Air quality affected by trees in real street canyons : the case of Marylebone neighbourhood in central London, *Urban for, Urban Green* 22 (2017) 41–53, <https://doi.org/10.1016/j.ufug.2017.01.009>.
- [36] K. V. Abhijith, P. Kumar, Field investigations for evaluating green infrastructure effects on air quality in open-road conditions, *Atmos. Environ.* 201 (2019) 132–147, <https://doi.org/10.1016/j.atmosenv.2018.12.036>.

- [37] A.P.R. Jeanjean, G. Hinchliffe, W.A. McMullan, P.S. Monks, R.J. Leigh, A CFD study on the effectiveness of trees to disperse road traffic emissions at a city scale, *Atmos. Environ.* 120 (2015) 1–14, <https://doi.org/10.1016/j.atmosenv.2015.08.003>.
- [38] E.S. Lee, D.R. Ranasinghe, F. Enayati, S. Amini, S. Mara, W. Choi, S. Paulson, Y. Zhu, Field evaluation of vegetation and noise barriers for mitigation of near-free-way air pollution under variable wind conditions, *Atmos. Environ.* 175 (2018) 92–99, <https://doi.org/10.1016/j.atmosenv.2017.11.060>.
- [39] M. Lin, G. Hagler, R. Baldauf, V. Isakov, H. Lin, A. Khlystov, The effects of vegetation barriers on near-road ultrafine particle number and carbon monoxide concentrations, *Sci. Total Environ.* 553 (2016) 372–379, <https://doi.org/10.1016/j.scitotenv.2016.02.035>.
- [40] S. Janhäll, Review on urban vegetation and particle air pollution - deposition and dispersion, *Atmos. Environ.* 105 (2015) 130–137, <https://doi.org/10.1016/j.atmosenv.2015.01.052>.
- [41] J. Gallagher, A modelling exercise to examine variations of NO<sub>x</sub> concentrations on adjacent footpaths in a street canyon: the importance of accounting for wind conditions and fleet composition, *Sci. Total Environ.* 550 (2016) 1065–1074, <https://doi.org/10.1016/j.scitotenv.2016.01.096>.
- [42] N. Schulte, M. Snyder, V. Isakov, D. Heist, A. Venkatram, Effects of solid barriers on dispersion of roadway emissions, *Atmos. Environ.* 97 (2014) 286–295, <https://doi.org/10.1016/j.atmosenv.2014.08.026>.
- [43] J.I. Huertas, J.E. Aguirre, O.D. Lopez Mejia, C.H. Lopez, Design of road-side barriers to mitigate air pollution near roads, *Appl. Sci.* 11 (2021) 1–20, <https://doi.org/10.3390/app11052391>.
- [44] S. Wang, X. Wang, Modeling and analysis of the effects of noise barrier shape and inflow conditions on highway automobiles emission dispersion, *Fluid 4* (2019).
- [45] C.M. Collins, A. Otero, H. Woodward, Shape matters: reducing people's exposure to poor air quality using sculpted infrastructure elements, *Cities Heal* (2021) 1–7, <https://doi.org/10.1080/23748834.2021.1883888>.
- [46] R.D. Bornstein, D.S. Johnson, Urban-rural wind velocity differences, *Atmos. Environ. Times* 11 (1977) 597–604.
- [47] A.M. Droste, G.J. Steeneveld, A.A.M. Holtslag, Introducing the urban wind island effect, *Environ. Res. Lett.* 13 (2018).
- [48] L. Wang, Q. Pan, X.P. Zheng, S.S. Yang, Effects of low boundary walls under dynamic inflow on flow field and pollutant dispersion in an idealized street canyon, *Atmos. Pollut. Res.* 8 (2017) 564–575, <https://doi.org/10.1016/j.apr.2016.12.004>.
- [49] A. McNabola, B.M. Broderick, L.W. Gill, A numerical investigation of the impact of low boundary walls on pedestrian exposure to air pollutants in urban street canyons, *Sci. Total Environ.* 407 (2009) 760–769, <https://doi.org/10.1016/j.scitotenv.2008.09.036>.
- [50] Z.T. Ai, C.M. Mak, CFD simulation of flow in a long street canyon under a perpendicular wind direction: evaluation of three computational settings, *Build. Environ.* 114 (2017) 293–306, <https://doi.org/10.1016/j.buildenv.2016.12.032>.
- [51] H.P.A.H. Irwin, The design of spires for wind simulation, *J. Wind Eng. Ind. Aerod.* 7 (1981) 361–366, [https://doi.org/10.1016/0167-6105\(81\)90058-1](https://doi.org/10.1016/0167-6105(81)90058-1).
- [52] G. Comte-Bellot, Hot-wire anemometry, *Annu. Rev. Fluid Mech.* 8 (1976) 209–231.
- [53] W.H. Snyder, *Guideline for Fluid Modeling of Atmospheric Diffusion*, Environmental Sciences Research Laboratory, Office of Research and Development, US Environmental Protection Agency, 1981.
- [54] Y. Lin, J. Hang, H. Yang, L. Chen, G. Chen, H. Ling, M. Sandberg, L. Claesson, C.K. C. Lam, Investigation of the Reynolds number independence of cavity flow in 2D street canyons by wind tunnel experiments and numerical simulations, *Build. Environ.* 201 (2021) 107965, <https://doi.org/10.1016/j.buildenv.2021.107965>.
- [55] L. Perret, J. Basley, R. Mathis, T. Piquet, The atmospheric boundary layer over urban-like terrain: influence of the plan density on roughness sublayer dynamics, *Boundary-Layer Meteorol.* 170 (2019) 205–234, <https://doi.org/10.1007/s10546-018-0396-9>.
- [56] P.J. Richards, R.P. Hoxey, Appropriate boundary conditions for computational wind engineering models using the k-ε turbulence model, *J. Wind Eng. Ind. Aerod.* 46 & 47 (1993) 145–153, <https://doi.org/10.1016/B978-0-444-81688-7.50018-8>.
- [57] C. Nironi, P. Salizzoni, M. Marro, P. Mejean, N. Grosjean, L. Soulhac, Dispersion of a passive scalar fluctuating plume in a turbulent boundary layer. Part I: velocity and concentration measurements, *Boundary-Layer Meteorol.* 156 (2015) 415–446, <https://doi.org/10.1007/s10546-015-0040-x>.
- [58] J.E. Fackrell, A.G. Robins, Concentration fluctuations and fluxes in plumes from point sources in a turbulent boundary layer, *J. Fluid Mech.* 117 (1982) 1–26.
- [59] P. Salizzoni, L. Soulhac, P. Mejean, R.J. Perkins, Influence of a two-scale surface roughness on a neutral turbulent boundary layer, *Boundary-Layer Meteorol.* 127 (2008) 97–110, <https://doi.org/10.1007/s10546-007-9256-8>.
- [60] V. Garbero, P. Salizzoni, L. Soulhac, Experimental study of pollutant dispersion within a network of streets, *Boundary-Layer Meteorol.* 136 (2010) 457–487, <https://doi.org/10.1007/s10546-010-9511-2>.
- [61] C.S.B. Grimmond, T.R. Oke, Aerodynamic properties of urban areas derived from analysis of surface form, *J. Appl. Meteorol. Climatol.* 38 (1999) 1262–1292, [https://doi.org/10.1175/1520-0450\(1999\)038<1262:APOUAD>2.0.CO;2](https://doi.org/10.1175/1520-0450(1999)038<1262:APOUAD>2.0.CO;2).
- [62] M.W. Rotach, Profiles of turbulence statistics in and above an urban street canyon, *Atmos. Environ. Times* 29 (1995) 1473–1486, [https://doi.org/10.1016/1352-2310\(95\)00084-C](https://doi.org/10.1016/1352-2310(95)00084-C).
- [63] P. Salizzoni, M. Marro, L. Soulhac, N. Grosjean, R.J. Perkins, Turbulent transfer between street canyons and the overlying atmospheric boundary layer, *Boundary-Layer Meteorol.* 141 (2011) 393–414, <https://doi.org/10.1007/s10546-011-9641-1>.
- [64] M.R. Raupach, R.A. Antonia, S. Rajagopalan, Rough-wall turbulent boundary layers, *Appl. Mech. Rev.* 44 (1991) 1–25.
- [65] J.M. Lewis, T.W. Koster, J.C. LaRue, On the determination of the dissipation rate of turbulence kinetic energy, *Exp. Fluid* 62 (2021) 1–13, <https://doi.org/10.1007/s00348-021-03243-2>.
- [66] G. Wang, F. Yang, K. Wu, Y. Ma, C. Peng, T. Liu, L.P. Wang, Estimation of the dissipation rate of turbulent kinetic energy: a review, *Chem. Eng. Sci.* 229 (2021), <https://doi.org/10.1016/j.ces.2020.116133>.
- [67] J.O. Hinze, *Turbulence*, second ed., 1975.
- [68] D. Marucci, M. Carpentieri, Effect of local and upwind stratification on flow and dispersion inside and above a bi-dimensional street canyon, *Build. Environ. Times* 156 (2019) 74–88, <https://doi.org/10.1016/j.buildenv.2019.04.013>.
- [69] J. Allegrini, V. Dorer, J. Carmeliet, Wind tunnel measurements of buoyant flows in street canyons, *Build. Environ.* 59 (2013) 315–326, <https://doi.org/10.1016/j.buildenv.2012.08.029>.
- [70] D. Guan, Y. Zhang, T. Zhu, A wind-tunnel study of windbreak drag, *Agric. For. Meteorol.* 118 (2003) 75–84, [https://doi.org/10.1016/S0168-1923\(03\)00069-8](https://doi.org/10.1016/S0168-1923(03)00069-8).
- [71] G. De-xin, Z. Ting-yao, H. Shi-jie, Wind tunnel experiment of drag of isolated tree macodels in surface boundary layer, *J. For. Res.* 11 (2000) 156–160, <https://doi.org/10.1007/bf02855516>.
- [72] L. Manickathan, T. Defraeye, J. Allegrini, D. Derome, J. Carmeliet, Comparative study of flow field and drag coefficient of model and small natural trees in a wind tunnel, *Urban For. Urban Green.* 35 (2018) 230–239, <https://doi.org/10.1016/j.ufug.2018.09.011>.
- [73] Y. Zhao, L. Wai Chew, Y. Fan, C. Gromke, J. Hang, Y. Yu, A. Ricci, Y. Zhang, Y. Xue, S. Fellini, P.A. Mirzaei, N. Gao, M. Carpentieri, P. Salizzoni, J. Niu, J. Carmeliet, Fluid tunnel research for challenges of urban climate, *Urban Clim.* 51 (2023) 101659, <https://doi.org/10.1016/j.uclim.2023.101659>.
- [74] R. Popek, A. Łukowski, P. Karolewski, Particulate matter accumulation - further differences between native *Prunus padus* and non-native *P. serotina*, *Dendrobiology* 78 (2017) 85–95, <https://doi.org/10.12657/denbio.078.009>.
- [75] T. Blanus, M. Garratt, M. Cathcart-James, L. Hunt, R.W.F. Cameron, Urban hedges: a review of plant species and cultivars for ecosystem service delivery in north-west Europe, *Urban for. Urban Green* 44 (2019) 126391, <https://doi.org/10.1016/j.ufug.2019.126391>.
- [76] M. Marro, H. Gamel, P. Méjean, H. Correia, L. Soulhac, P. Salizzoni, High-frequency simultaneous measurements of velocity and concentration within turbulent flows in wind-tunnel experiments, *Exp. Fluid* 61 (2020) 1–13, <https://doi.org/10.1007/s00348-020-03074-7>.
- [77] R.N. Meroney, M. Pavageau, S. Rafailidis, M. Schatzmann, Study of line source characteristics for 2-D physical modelling of pollutant dispersion in street canyons, *J. Wind Eng. Ind. Aerod.* 62 (1996) 37–56, [https://doi.org/10.1016/S0167-6105\(96\)00057-8](https://doi.org/10.1016/S0167-6105(96)00057-8).
- [78] M. Pavageau, M. Schatzmann, Wind tunnel measurements of concentration fluctuations in an urban street canyon, *Atmos. Environ. Times* 33 (1999) 3961–3971, [https://doi.org/10.1016/S1352-2310\(99\)00138-7](https://doi.org/10.1016/S1352-2310(99)00138-7).
- [79] M.F. Yassin, M. Ohba, Experimental simulation of air quality in street canyon under changes of building orientation and aspect ratio, *J. Expo. Sci. Environ. Epidemiol.* 22 (2012) 502–515, <https://doi.org/10.1038/jes.2012.59>.
- [80] C. Vidali, M. Marro, H. Correia, L. Gostiaux, S. Jallais, D. Houssin, E. Vyazmina, P. Salizzoni, Wind-tunnel experiments on atmospheric heavy gas dispersion: meteorological aspects, *Exp. Therm. Fluid Sci.* 130 (2022) 110495, <https://doi.org/10.1016/j.expthermflsci.2021.110495>.
- [81] A. Lewis, S.J. Moller, D. Carslaw, *Impacts of Vegetation on Urban Air Pollution*, 2018.
- [82] K. Hashad, B. Yang, R.W. Baldauf, P. Deshmukh, V. Isakov, K.M. Zhang, Enhancing the local air quality benefits of roadside green infrastructure using low-cost, impermeable, solid structures (LISS), *Sci. Total Environ.* 717 (2020) 137136, <https://doi.org/10.1016/j.scitotenv.2020.137136>.
- [83] X. Jin, L. Yang, X. Du, Y. Yang, Transport characteristics of PM<sub>2.5</sub> inside urban street canyons: the effects of trees and vehicles, *Build. Simulat.* 10 (2017) 337–350, <https://doi.org/10.1007/s12273-016-0324-1>.
- [84] T. Oke, Street design and urban canopy layer climate, *Energy Build.* 1–3 (1988) 103–113, <https://doi.org/10.3109/08830189709116841>.
- [85] L.J. Hunter, I.D. Watson, G.T. Johnson, Modelling air flow regimes in urban canyons, *Energy Build.* 15 (1990) 315–324, [https://doi.org/10.1016/0378-7788\(90\)90004-3](https://doi.org/10.1016/0378-7788(90)90004-3).
- [86] G.T. Johnson, L.J. Hunter, Some insights into typical urban canyon airflows, *Atmos. Environ. Times* 33 (1999) 3991–3999, [https://doi.org/10.1016/S1352-2310\(99\)00164-8](https://doi.org/10.1016/S1352-2310(99)00164-8).
- [87] M. Marro, C. Nironi, P. Salizzoni, L. Soulhac, Dispersion of a passive scalar fluctuating plume in a turbulent boundary layer. Part II: analytical modelling, *Boundary-Layer Meteorol.* 156 (2015) 447–469, <https://doi.org/10.1007/s10546-015-0041-9>.
- [88] M. Marro, P. Salizzoni, L. Soulhac, M. Cassiani, Dispersion of a passive scalar fluctuating plume in a turbulent boundary layer. Part III: stochastic modelling, *Boundary-Layer Meteorol.* 167 (2018) 349–369, <https://doi.org/10.1007/s10546-017-0330-6>.
- [89] V. Fuka, Z.T. Xie, I.P. Castro, P. Hayden, M. Carpentieri, A.G. Robins, Scalar fluxes near a tall building in an aligned array of rectangular buildings, *Boundary-Layer Meteorol.* 167 (2018) 53–76, <https://doi.org/10.1007/s10546-017-0308-4>.
- [90] N. Ben Salem, V. Garbero, P. Salizzoni, G. Lamaison, L. Soulhac, Modelling pollutant dispersion in a street network, *Boundary-Layer Meteorol.* 155 (2015) 157–187, <https://doi.org/10.1007/s10546-014-9990-7>.

- [91] L. Soulhac, V. Garbero, P. Salizzoni, P. Mejean, R.J. Perkins, Flow and dispersion in street intersections, *Atmos. Environ.* 43 (2009) 2981–2996, <https://doi.org/10.1016/j.atmosenv.2009.02.061>.
- [92] A. Robins, E. Savory, A. Scaperdas, D. Grigoriadis, Spatial variability and source-receptor relations at a street intersection, *Urban Air Qual. — Recent Adv.* (2002) 381–393, [https://doi.org/10.1007/978-94-010-0312-4\\_27](https://doi.org/10.1007/978-94-010-0312-4_27).
- [93] Z. Li, H. Zhang, C.Y. Wen, A.S. Yang, Y.H. Juan, The effects of lateral entrainment on pollutant dispersion inside a street canyon and the corresponding optimal urban design strategies, *Build. Environ.* 195 (2021) 107740, <https://doi.org/10.1016/j.buildenv.2021.107740>.
- [94] L.J. Hunter, G.T. Johnson, I.D. Watson, An investigation of three-dimensional characteristics of flow regimes within the urban canyon, *Atmos. Environ. Times Part B, Urban Atmos.* 26 (1992) 425–432, [https://doi.org/10.1016/0957-1272\(92\)90049-X](https://doi.org/10.1016/0957-1272(92)90049-X).
- [95] W.G. Hoydysh, W.F. Dabberdt, Concentration fields at urban intersections: fluid modeling studies, *Atmos. Environ.* 28 (1994) 1849–1860.
- [96] A. Scaperdas, R.N. Colville, Assessing the Representativeness of Monitoring Data from an Urban Intersection Site in Central London, UK, n.d.
- [97] R. Buccolieri, M. Sandberg, S. Di Sabatino, City breathability and its link to pollutant concentration distribution within urban-like geometries, *Atmos. Environ.* 44 (2010) 1894–1903, <https://doi.org/10.1016/j.atmosenv.2010.02.022>.
- [98] M. Tomson, P. Kumar, Y. Barwise, P. Perez, H. Forehead, K. French, L. Morawska, J.F. Watts, Green infrastructure for air quality improvement in street canyons, *Environ. Int.* 146 (2021) 106288, <https://doi.org/10.1016/j.envint.2020.106288>.
- [99] S. Di Sabatino, R. Buccolieri, G. Pappacogli, L.S. Leo, The effects of trees on micrometeorology in a real street canyon: consequences for local air quality, *Int. J. Environ. Pollut.* 58 (2015) 100–111, <https://doi.org/10.1504/IJEP.2015.076587>.
- [100] C. Wang, Q. Li, Z.H. Wang, Quantifying the impact of urban trees on passive pollutant dispersion using a coupled large-eddy simulation–Lagrangian stochastic model, *Build. Environ.* 145 (2018) 33–49, <https://doi.org/10.1016/j.buildenv.2018.09.014>.
- [101] D. Hamlyn, R. Britter, A numerical study of the flow field and exchange processes within a canopy of urban-type roughness, *Atmos. Environ.* 39 (2005) 3243–3254, <https://doi.org/10.1016/j.atmosenv.2005.02.020>.
- [102] Y. Tominaga, T. Stathopoulos, CFD simulation of near-field pollutant dispersion in the urban environment: a review of current modeling techniques, *Atmos. Environ.* 79 (2013) 716–730, <https://doi.org/10.1016/j.atmosenv.2013.07.028>.